NEUROSCIENCE

Regulation of autism-related self-injurious behavior by electrical stimulation of corticostriatal circuits in mice and humans

Kristina Zhang[1,2], Jurgen Germann[3], Rafi Matin[1,2], Karim Mithani[2,4], Jacob Ellegood[5,6], Hrishikesh Suresh[2,4], Sammi Wong[5], Jason P. Lerch[5,7,8], Brian J. Nieman[5,7,9], Margot J. Taylor[2,10,11,12], Sara Breitbart[4], Alfonso Fasano[1,3], Carolina Gorodetsky[13], Flavia Venetucci Gouveia[2,5,9]*†, George M. Ibrahim[1,2,4]*†

Dysfunction of corticostriatal circuitry is related to the emergence of self-injurious behavior (SIB) in autism spectrum disorder (ASD). Despite mounting interest in circuit-based interventions for severe, refractory SIB, the lack of causal evidence linking modulation of corticostriatal networks to changes in SIB has limited the advancement of effective, targeted therapies. In this study, we demonstrate that electrical stimulation of the nucleus accumbens (NAcc) mitigates SIB and induces structural changes along corticostriatal circuits in a mouse model relevant for ASD and children with severe SIB undergoing NAcc-targeted deep brain stimulation. In BTBR T^{+} *Itpr3*^{tf}/J mice, NAcc stimulation selectively reduced injurious self-grooming—a behavioral metric of SIB—and led to morphological changes in corticostriatal networks. In children with severe SIB, electric stimulation at a locus of optimal therapeutic response within the NAcc engaged widespread sensorimotor, limbic, and striatal networks and induced longitudinal structural changes in fronto-limbic-striatal brain regions. These findings highlight the role of the fronto-limbic-striatal network in SIB regulation and support corticostriatal neuromodulation as a mechanistic therapy for these extreme behaviors.

INTRODUCTION

Corticostriatal circuits govern restricted and repetitive behaviors in autism spectrum disorder (ASD), which in their most extreme manifestation result in self-injurious behavior (SIB) (*1*, *2*). These behaviors are characterized by repetitive, stereotyped movements directed toward oneself that result in physical injury without suicidal intent (*3*, *4*). They typically emerge in childhood, persist into adulthood, and can cause irreversible injury or death, severely diminishing quality of life for both patients and their caregivers (*5*, *6*). While the majority of these behaviors respond to behavioral therapy, approximately 20 to 25% of SIB is invariant to environmental condition, refractory to intervention, and is presumed to be regulated by stronger neurobiological contributions (*4*). The lack of mechanistic understanding of the neural circuitry underlying SIB in ASD limits opportunities for circuit-informed interventions.

In both rodents and humans, the striatum functions as a key integrative node for the initiation and regulation of behavior (*7*). It receives convergent excitatory inputs from the cortex, thalamus, and limbic regions, along with dopaminergic afferents from the substantia nigra and ventral tegmental area (*7*–*9*). These integrated signals form the basis of corticostriatal circuitry—an interconnected network in which cortical projections converge on the striatum and are relayed through basal ganglia-thalamo-cortical loops to govern action selection, behavioral inhibition, and reward-based learning (*10*, *11*). By integrating these widespread cortical and subcortical inputs, the striatum contributes to many cognitive-behavioral functions that are characteristically altered in ASD, including motor and reward processing (*10*, *12*, *13*). Dysfunction within corticostriatal pathways has been implicated in the emergence of SIB and related phenotypes including stereotypy, impulsivity, and tics (*2*, *14*–*17*), which may share underlying pathophysiology involving impaired behavioral inhibition (*18*, *19*).

Large-scale projections of the striatum to frontal and limbic networks are thought to modulate repetitive behaviors. Individuals with ASD who exhibit high levels of repetitive behaviors show greater functional connectivity between the striatum and limbic structures of the medial temporal lobe compared to typically developing individuals (*20*, *21*). This hyperconnectivity is often accompanied by reduced connectivity between the striatum and frontal cortical areas, namely the prefrontal cortex (PFC), anterior cingulate cortex (ACC), and supplementary motor area (SMA) (*21*–*23*). Heightened limbic-striatal interactions, together with diminished frontostriatal connectivity, are thought to contribute to the expression of restricted and repetitive behaviors by impairing top-down inhibitory mechanisms that typically suppress such actions (*17*, *24*). In accordance with this, rodent models of repetitive, stereotyped, and compulsive behavior demonstrate hyperactivity in striatal interneurons and heightened excitatory input from frontal cortical projections (*25*, *26*). Changes in restricted and repetitive behaviors have also been linked

[1]Institute of Medical Science, University of Toronto, Toronto, Ontario, Canada. [2]Neurosciences and Mental Health, The Hospital for Sick Children, Toronto, Ontario, Canada. [3]Krembil Brain Institute, University Health Network, Toronto, Ontario, Canada. [4]Division of Neurosurgery, The Hospital for Sick Children, Toronto, Ontario, Canada. [5]Mouse Imaging Centre, The Hospital for Sick Children, Toronto, Ontario, Canada. [6]Bloorview Research Institute, Holland Bloorview Kids Rehabilitation Hospital, Toronto, Ontario, Canada. [7]Department of Medical Biophysics, University of Toronto, Toronto, Ontario, Canada. [8]Oxford Centre for Integrative Neuroimaging, Nuffield Department of Clinical Neuroscience, University of Oxford, Oxford, UK. [9]Translational Medicine, The Hospital for Sick Children, Toronto, Ontario, Canada. [10]Diagnostic and Interventional Radiology, The Hospital for Sick Children, Toronto, Ontario, Canada. [11]Department of Medical Imaging, University of Toronto, Toronto, Ontario, Canada. [12]Department of Psychology, University of Toronto, Toronto, Ontario, Canada. [13]Division of Neurology, The Hospital for Sick Children, Toronto, Ontario, Canada.
*Corresponding author. Email: george.ibrahim@sickkids.ca (G.M.I.); flavia.venetuccigouveia@sickkids.ca (F.V.G.)
†These authors contributed equally to this work.

to structural alterations and lesions within medial temporal lobe structures, including the amygdalae, hippocampi, and limbic-associated cortices (i.e., cingulate cortex, insula, and entorhinal cortex), which are critically involved in emotional salience and behavior control (*23*, *27*–*29*).

Within corticostriatal circuitry, the nucleus accumbens (NAcc) of the ventral striatum serves as a major convergence point for projections from both frontal and limbic regions, positioning it as the main input nucleus of the basal ganglia (*14*). By integrating executive and motor signals from the PFC with emotional and contextual information from the amygdalae and hippocampi, the NAcc is well-positioned to regulate the automatic maintenance of repetitive or SIBs (*10*, *13*, *14*). In humans, repetitive behaviors in ASD have been associated with accelerated postnatal growth of the ventral striatum, including the NAcc (*13*, *28*). In animal studies, focal lesions to the NAcc have shown to increase impulsivity (*30*–*33*), while optogenetic manipulation of the NAcc or its extended striatal projections modulates the frequency and severity of compulsive and reward-driven behaviors (*34*–*39*). Specifically, optogenetic inhibition of projections from temporal lobe structures, such as the basolateral amygdala, to the NAcc has been shown to attenuate compulsive reward-seeking behavior in rodents (*38*–*40*). Conversely, chemogenetic and optogenetic stimulation of frontostriatal pathways involving the NAcc suppresses repetitive and reward-seeking behaviors (*35*–*37*).

Building on these preclinical insights, prior clinical attempts to mitigate SIB in ASD and related disorders have used neuromodulation through deep brain stimulation (DBS) of subcortical targets, including the basolateral amygdala (*41*), globus pallidus (*42*), and posterior hypothalamus (*43*). While these sites are implicated in emotional reactivity and motor output, evidence for their efficacy as DBS targets remains limited and therapeutic outcomes have been variable (*44*, *45*). Direct comparisons of these targets are scarce; however, recent network-level analyses suggest that the therapeutic effects of these disparate targets may converge on a common limbic-striatal network anchored by the ventral striatum, particularly the NAcc (*44*). Situated at the intersection of prefrontal executive control, limbic emotional regulation, and reward processing, the NAcc is uniquely positioned to modulate behavioral inhibition—a process central to repetitive behavior and SIB.

Despite extensive investigations, direct causal evidence linking corticostriatal pathways to SIB in humans remains elusive. Furthermore, while electrical stimulation presents a means to modulate brain circuits through DBS, its potential effect on corticostriatal circuits that regulate SIB is not known. To address this gap, we evaluated the effects of targeted electrical stimulation of the NAcc on corticostriatal networks and maintenance of SIB in ASD. Leveraging a cross-species approach, we used the BTBR T^{+} $Itpr3^{tf}$/J (BTBR) mouse model relevant to ASD and longitudinal data from the first-in-human clinical trial of NAcc-targeted DBS (NAcc-DBS) in children with ASD and severe, refractory SIB [ClinicalTrials.gov, NCT03982888; (*46*)]. The inbred BTBR mouse exhibits core ASD-related behavior deficits, most notably, spontaneously elevated levels of repetitive self-grooming that leads to physical injury—a behavior comparable to SIB in humans (*47*–*49*). We first show that electric stimulation of the NAcc selectively reduces SIB and repetitive behavior in BTBR mice through morphological alteration of fronto-limbic-striatal structures. We then evaluate brain-wide circuitry changes involved in SIB regulation in human participants undergoing NAcc-DBS and show that SIB improvement is associated with engagement of sensorimotor, limbic, and striatal networks. Closing this translational circle, we identify longitudinal structural alterations in homologous fronto-limbic-striatal regions in both BTBR mice and human participants undergoing NAcc modulation, highlighting conserved circuit-level mechanisms underlying the regulation of SIB in ASD.

RESULTS

Effects of NAcc electrical stimulation on behavior in an ASD mouse model

We tested the hypothesis that targeted electrical stimulation of the NAcc would attenuate the severity and duration of SIB (i.e., injurious self-grooming) and repetitive behaviors in BTBR mice by engaging corticostriatal regions. We delivered chronic high-frequency electrical stimulation (5 hours/day, 4 days; 100 μA, 100 Hz, 60 μs) to the bilateral NAcc via stereotactically implanted electrodes (Fig. 1, A to C; see Materials and Methods). BTBR mice were randomized into three groups: DBS-ON ($n = 10$), which received active NAcc electrical stimulation; DBS-OFF ($n = 10$), which were implanted with NAcc electrodes but received no stimulation; and Control ($n = 14$), which were neither implanted nor stimulated. Table S1 provides a detailed summary of behavioral outcomes for all groups and test sessions.

To test the effects of NAcc electric stimulation on SIB, we evaluated self-grooming frequency, severity, and extent of resulting physical injury in BTBR mice. While the Control group could be visually distinguished because of the absence of an implant cap, behavioral and physical injury ratings were blinded between the DBS-ON and DBS-OFF groups. Physical injury was quantified as the proportion of dorsal body surface area exhibiting hair loss and skin lesioning due to excessive self-grooming, measured before and after the stimulation period. Mice that received NAcc electrical stimulation exhibited an average decrease in surface area of physical injury over the dorsal body relative to baseline, which differed significantly from DBS-OFF ($F_{2,31} = 6.57$, $P < 0.01$) and Control ($F_{2,31} = 6.57$, $P < 0.05$; Fig. 1, D and E) mice, wherein physical injury increased. In contrast to DBS-OFF mice, which showed a significant increase in time spent self-grooming relative to baseline ($F_{1,18} = 8.42$, $P < 0.01$), DBS-ON mice maintained grooming duration close to baseline levels ($F_{2,31} = 4.77$, $P < 0.05$; Fig. 1F). To further assess the effect of NAcc stimulation on SIB-related activity, we analyzed grooming pattern, measured by the proportion of correct transitions through syntactic self-grooming phases (*50*). BTBR mice are known to exhibit markedly disrupted syntactic grooming organization, characterized by incorrect grooming phase transitions that reflect stereotyped and rigid grooming patterns (*51*). DBS-ON mice exhibited a significantly greater increase in the proportion of correct grooming transitions relative to DBS-OFF ($F_{2,31} = 4.27$, $P < 0.05$) and Control ($F_{2,31} = 4.27$, $P < 0.01$; Fig. 1G). Self-grooming (i.e., duration and pattern) was scored by two experienced raters [duration: intraclass correlation coefficient (ICC) = 0.99, $P = 2.0 \times 10^{-20}$; pattern: ICC = 0.93, $P = 4.4 \times 10^{-10}$; fig. S1]. More severe repetitive behaviors are considered risk factors for SIB (*19*). DBS-ON mice demonstrated significantly reduced repetitive behaviors together with reductions in SIB, measured by repetitive marble-burying ($F_{2,30} = 6.10$, $P < 0.01$; Fig. 1H).

The behavioral effects of NAcc stimulation were specific to SIB and repetitive behaviors, with no effect detected in anxiety-like behavior, locomotor activity, or social interaction. The open field test

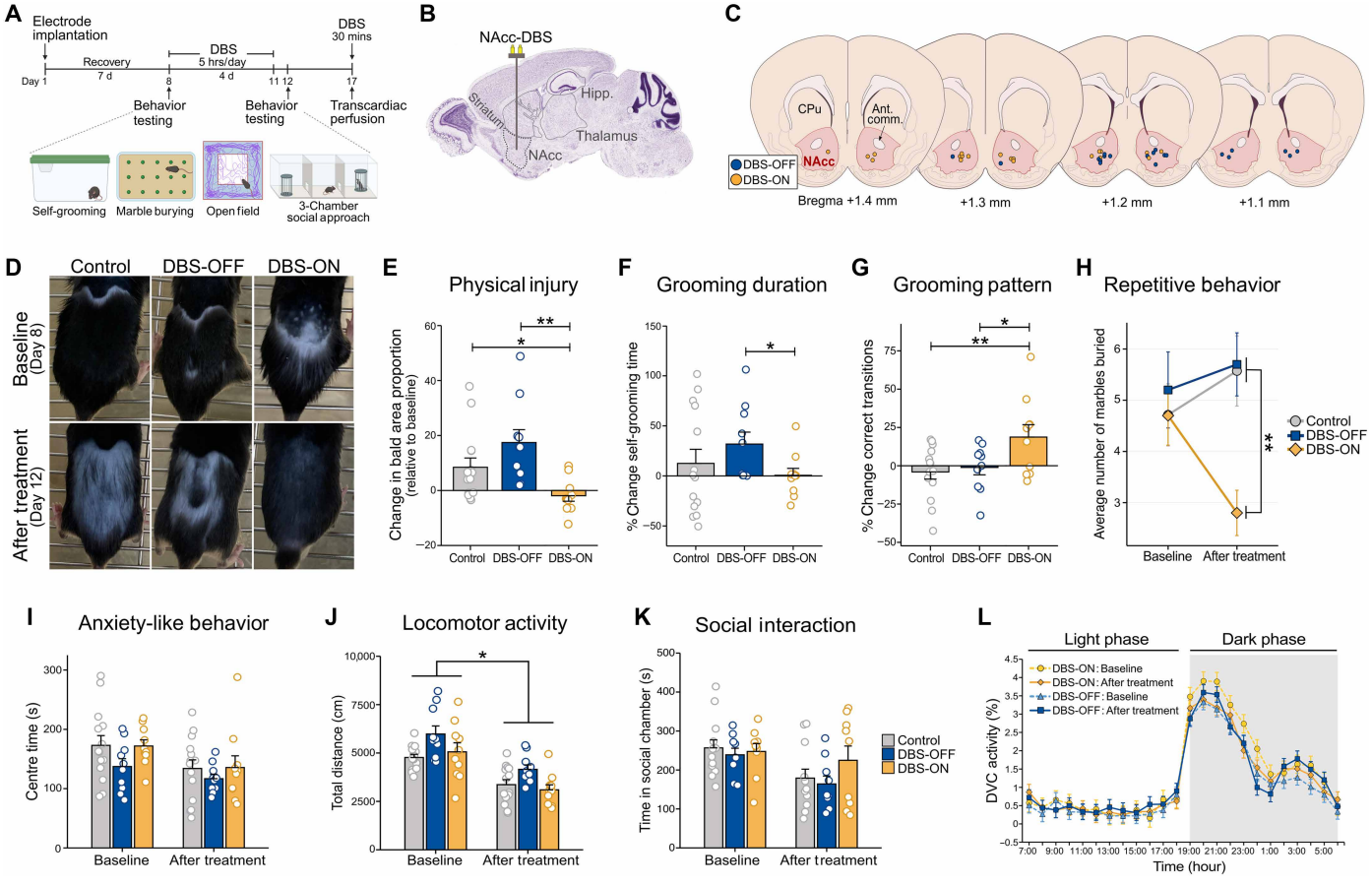

Fig. 1. Behavior testing paradigms and stimulation outcomes. (**A**) Experimental timeline. Created in BioRender. Zhang, K. (2025) https://BioRender.com/kio8ee4. (**B**) Schematic depicting DBS electrodes in the NAcc. Nissl image from Allen Reference Atlas–Mouse Brain (*132*). (**C**) Localization of electrode tips in the NAcc (red) of DBS-OFF (blue) and DBS-ON (yellow). (**D**) Representative images of Control ($n = 14$), DBS-OFF ($n = 10$), and DBS-ON ($n = 10$) mouse body before and after NAcc stimulation period. (**E**) Change in proportion of physically injured bald area relative to baseline. (**F**) Percentage change of grooming time (measured in seconds) and (**G**) correct transitions through syntactic grooming phases (*50*) during grooming assay, relative to baseline. Statistics for (E) to (G) analyzed by linear regression. (**H**) Mean number of marbles buried in the marble-burying test. (**I**) Time in center zone (measured in seconds; $P = 0.91$) and (**J**) total distance traveled (measured in centimeters) in the open field test. (**K**) Time in social chamber (measured in seconds; $P = 0.24$) in the three-chamber social approach test. (**L**) Activity index across time points in the light (unshaded) and dark (shaded) phases, measured using the DVC system. The activity index is calculated on the basis of changes in electrical capacitance caused by the animal's movement across the cage floor, with higher changes indicating more activity (*53*). Statistics for (H) to (K) analyzed by linear mixed-effect models. Data are shown as means ± SEM; $^*P < 0.05$, $^{**}P < 0.01$. For detailed behavior measures, see table S1. Ant. comm., anterior commissure; CPu, caudoputamen; d, days; DBS, deep brain stimulation; Hipp., hippocampus; hrs, hours; NAcc, nucleus accumbens.

showed no significant effect of NAcc electric stimulation on time spent in the center of the field ($\beta = -2.62$, $P = 0.91$; Fig. 1I) or total distance traveled ($\beta = 561.50$, $P = 0.15$; Fig. 1J) between groups. All groups demonstrated a significant decrease in overall distance traveled within the open field after the NAcc stimulation period when compared to baseline ($\beta = -1964.37$, $P < 0.0001$). However, no differences were reported in the total distance traveled and other movement characteristics such as velocity ($\beta = 0.05$, $P = 0.98$), vertical activity ($\beta = 28.4$, $P = 0.47$), and clockwise rotations ($\beta = 7.30$, $P = 0.08$) across groups and time points, demonstrating that NAcc electrical stimulation did not affect movement quality among stimulated animals. While the reduction in distance traveled between test sessions may be attributable to habituation to the open field arena (*52*), the absence of group differences in total distance and movement quality at each time point supports the specificity of NAcc electrical stimulation in modulating SIB without inducing adverse or nonspecific locomotor alterations.

The three-chamber social approach test also showed no significant effect of NAcc electric stimulation on time spent in the social chamber between groups ($\beta = -55.20$, $P = 0.24$; Fig. 1K). We further analyzed behavior patterns through continuous recording of circadian activity using the digital ventilated cage (DVC) system (*53*). No differences were observed for home-cage locomotor activity across groups and time points ($\beta = -8.99 \times 10^{-3}$, $P = 0.46$; Fig. 1L). Together, these data demonstrate that modulation of corticostriatal circuitry through the NAcc reduces SIB and repetitive behavior without affecting anxiety-like behavior, locomotion, and circadian patterns of BTBR mice.

Analysis of ASD mouse brain structure after NAcc-DBS via MRI

To study structural changes induced by chronic electrical stimulation of the NAcc, we performed deformation-based morphometry (DBM) using ex vivo structural magnetic resonance imaging (MRI)

captured from BTBR mice after the experimental stimulation period. We quantified brain structure in terms of regional volumetric expansion or contraction using the Jacobian determinants of the deformation field derived from a series of linear and nonlinear registrations (*54*). Two measurements were calculated to assess the volume in DBS-ON brain as compared to DBS-OFF: absolute volume (cubic millimeter), providing a direct measure of regional structural size and reflecting the sum of local microscale properties, and relative volume (percentage of the total brain volume), representing the proportional contribution of each region to overall brain size and capturing its scaling relationship with the whole brain. Total brain volume did not differ significantly between DBS-ON and DBS-OFF groups ($F_{2,30} = 4.90$, $P = 0.31$). Thus, absolute volumes were used to assess the regional volumetric changes, and relative volume differences can be found in fig. S2.

Voxel-wise analyses revealed significant absolute volume differences between DBS-ON and DBS-OFF groups across multiple regions within the fronto-limbic-striatal circuit. Compared to DBS-OFF, DBS-ON mice exhibited robust volume reduction in the striatum ($F_{1,17} = 11.71$, $P < 0.01$), globus pallidus ($F_{1,17} = 6.80$, $P < 0.05$), parietotemporal cortex ($F_{1,17} = 11.00$, $P < 0.01$), thalamus ($F_{1,17} = 4.80$, $P < 0.05$), and hippocampi ($F_{1,17} = 14.36$, $P < 0.01$; Fig. 2A). Further network-wide alterations were detected in structures that can be categorized into three interconnected regions: (i) frontal cortex (primary somatosensory cortex, supplemental somatosensory area, SMA, and ACC), (ii) limbic system (amygdala, hypothalamus, habenula, subiculum, entorhinal cortex, and bed nucleus of the stria terminalis), and (iii) striatum (caudoputamen and globus pallidus externa) (Fig. 2B). Several of these regions showed bilateral alterations, particularly in limbic structures such as the amygdalae, hippocampi, thalamus, and habenula, which are known to interact with the striatum via limbic-striatal projections (*7*–*9*). A full summary of affected regions is presented in table S2, defined using the Dorr-Steadman-Ullman-Richards-Qiu-Egan 40-μm mouse brain atlas (*55*).

To examine anatomical-behavioral relations, we tested whether structural variation in these fronto-limbic-striatal regions correlated with individual differences in SIB and repetitive behavior in BTBR mice. We identified significant associations between measures of SIB and/or repetitive behavior and spatially contiguous groups of voxels showing significant volume differences—referred to as clusters—within fronto-limbic-striatal structures (table S3). Time spent self-grooming was positively correlated with the absolute volume of clusters within the striatum [coefficient of determination (R^2) = 0.392, $q_{FDR} = 0.048$], globus pallidus ($R^2 = 0.356$, $q_{FDR} = 0.051$), and parietotemporal cortex ($R^2 = 0.366$, $q_{FDR} = 0.051$), which are known to be associated with reinforcing reward mechanisms (Fig. 2C) (*7*, *56*). Larger cluster volumes in the striatum ($R^2 = 0.346$, $q_{FDR} = 0.052$), thalamus ($R^2 = 0.376$, $q_{FDR} = 0.055$), and hippocampi ($R^2 = 0.371$, $q_{FDR} = 0.051$) were associated with repetitive marble-burying, indicating a positive relation between regional volume and repetitive behavior in BTBR mice (Fig. 2D). These anatomical-behavioral correlations were significant at the uncorrected level ($P < 0.05$), with the association between striatal cluster volume and self-grooming time remaining significant after correction for multiple comparisons. The remaining correlations approached, but did not exceed, the false discovery rate (FDR)–corrected significance threshold ($q_{FDR} < 0.05$). Representative MRI sections highlight structural differences in the striatum between a mouse with high levels of injurious self-grooming and low levels of injurious self-grooming (Fig. 2E).

These findings demonstrate that chronic electrical stimulation of the NAcc induces widespread volumetric alterations within fronto-limbic-striatal circuits implicated in sensorimotor integration and motor control. Volume differences in specific frontal, limbic, and parietotemporal regions of DBS-ON mice were associated with lower levels of SIB and repetitive behavior, suggesting that structural alterations within the fronto-limbic-striatal network may underlie the behavioral effects of corticostriatal modulation in BTBR mice.

Probabilistic mapping in children with SIB during NAcc-DBS

Next, we investigated whether modulation of corticostriatal circuitry similarly exerts brain-wide structural changes in children with profound ASD and severe SIB. We leveraged clinical and neuroimaging data collected from a first-in-human phase 1 trial of children with severe SIB who received NAcc-DBS [ClinicalTrials.gov, NCT03982888; (*46*)]. Six pediatric participants (three males and three females; 10.5 ± 1.2 years of age ranging from 7 to 14 years) underwent NAcc-DBS and were monitored for 1 year to assess treatment safety, feasibility, and behavioral outcomes. Clinical change in SIB was measured by the difference in Repetitive Behavior Scale–Revised [RBS–R; (*57*)] SIB subscore at baseline and 1-year follow-up for each participant. Table S4 summarizes the participant demographics and stimulation parameters applied.

Five of the 6 participants demonstrated significant improvement in SIB and quality of life after 1 year of NAcc-DBS, as indexed by the RBS-R SIB subscore and Pediatric Quality of Life Inventory, respectively (Table 1). On average, there was a 44.3% reduction in SIB and 141.5% improvement in health-related quality of life following NAcc-DBS. The one child who did not exhibit an improvement in SIB or quality of life presented with abnormal intracranial findings at baseline, including agenesis of the corpus callosum and associated colpocephaly consistent with a known history of in utero exposure to alcohol and substances.

We first sought to understand whether stimulation of subregions of the NAcc was preferentially associated with greater behavioral regulation. Using pre- and postoperative T1-weighted MRIs, we confirmed that electrodes were localized within the NAcc region in all participants, with the distal-most contact of the leads placed at the ventral margin of the NAcc and the proximal-most contact within the anterior limb of the internal capsule (Fig. 3A). By mapping the stimulation amplitude and frequency for each participant, we modeled each subject's volume of activated tissue (VAT) after 1 year of treatment (Fig. 3B), which reflects the brain volume influenced by the voltage field (*58*). Probabilistic voxel efficacy mapping (fig. S3; see Materials and Methods) revealed greater SIB reduction with stimulation of the posterior-inferior-lateral subregion of the NAcc (Fig. 3, C and D). The centroid of this sweet-spot localized to MNI152 space at coordinates $x = \pm 11$, $y = 6$, and $z = -12$ (https://www.bic.mni.mcgill.ca/ServicesAtlases/ICBM152NLin2009) and in Talairach-Tournoux space at coordinates $x = \pm 10$, $y = 3$, and $z = -7$ (http://talairach.org/). Relative to the anterior commissure, the sweet-spot was located at $x = \pm 10.5$ mm, $y = +3.5$ mm, and $z = +6.5$ mm from the midline of the anterior commissure.

Functional and structural connectivity patterns of NAcc-DBS in children with SIB

We next investigated large-scale circuits engaged by NAcc-DBS and associated with SIB improvement in participants using normative structural and functional connectivity mapping. To study large-scale

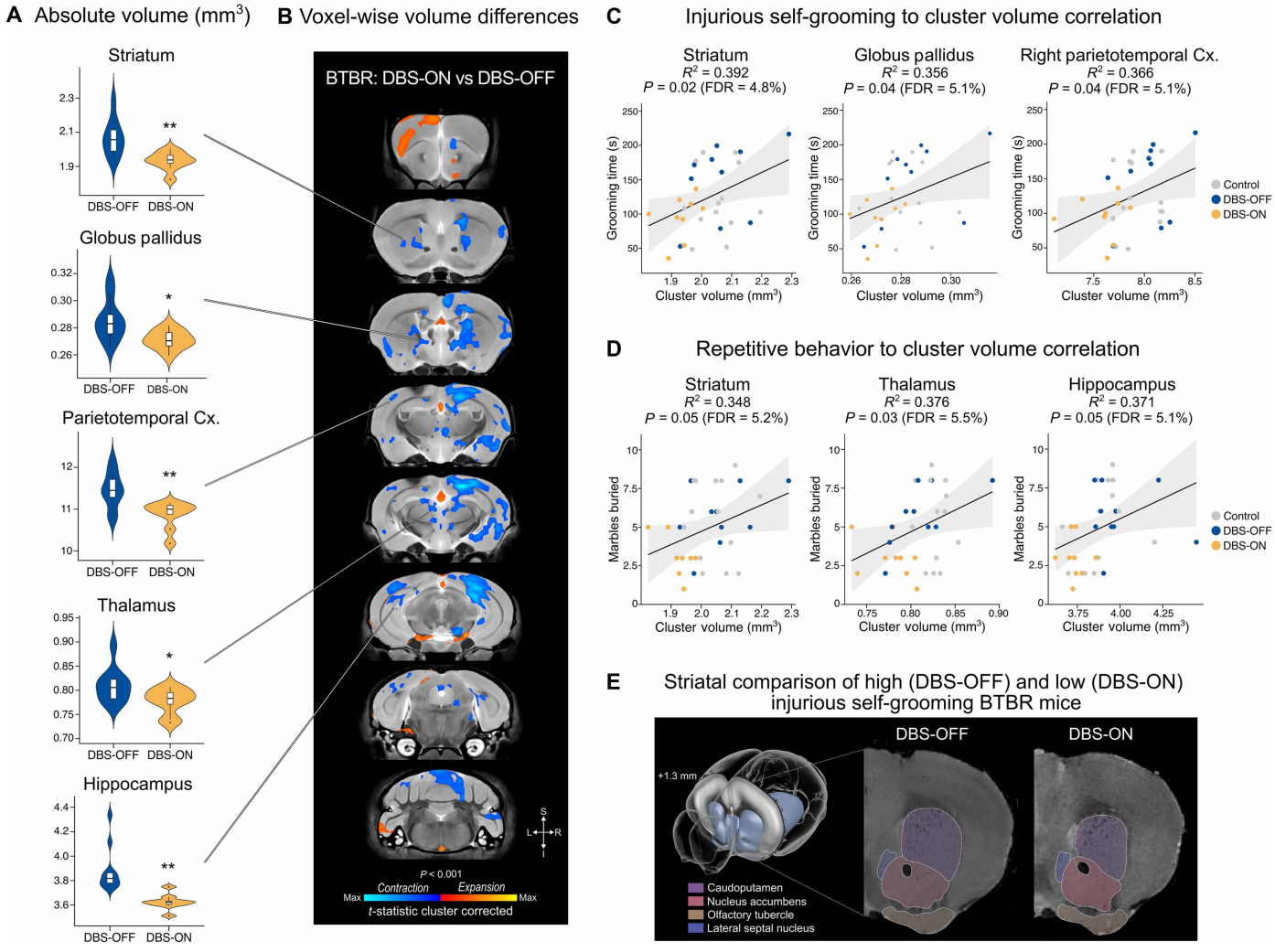

Fig. 2. Volumetric alterations in ASD mouse model after NAcc electrical stimulation. (**A**) Differences in absolute volume of significant clusters by region. Violin outline width represents density. Box: 1st quartile, median, 3rd quartile; whiskers: ±1.5 * IQR. *$P < 0.05$, **$P < 0.01$, linear regression. The absolute cluster volume represents the volume of significantly affected voxel clusters within each respective structure. (**B**) Voxel-wise absolute volume differences between DBS-ON and DBS-OFF. Warm colors represent significantly larger areas in the DBS-ON compared to DBS-OFF and cool colors represent significantly smaller areas in DBS-ON mice. All changes highlighted are significant at a cluster-forming threshold of $P < 0.05$ and size threshold of $P < 0.001$. (**C**) Relationship of cluster volume and time spent self-grooming. Three specific regions that are relevant to injurious self-grooming are highlighted: striatum, globus pallidus, and right parietotemporal cortex. (**D**) Concordance of cluster volume and repetitive behavior (marble-burying). Three specific regions that are relevant to repetitive behavior are highlighted: striatum, thalamus, and hippocampus. Cluster volume represents the volume of clusters of significantly affected voxels within each structure. Shaded gray area represents the 95% confidence interval. (**E**) Representative coronal MRI sections (bregma: +1.3 mm) showing striatal structure in a DBS-OFF mouse with high levels of injurious self-grooming (left) and a DBS-ON mouse with low injurious self-grooming (right). The light blue region in the three-dimension brain depicts the striatum, generated using the Scalable Brain Atlas (*133*). BTBR, BTBR T^{+} *Itpr3*^{tf}/J; Cx., cortex; FDR, false discovery rate.

structural networks modulated by NAcc-DBS, we mapped each participants' VAT to underlying brain circuits by identifying all discriminative streamlines intersecting the individual VATs within a whole-brain tractography template comprising ~12 million streamlines [see Materials and Methods; (*59*)].

The highest density of fiber tracts associated with improvement in RBS-R SIB subscore engaged the anterior commissure (Fig. 4, A and B; $q_{FDR} < 0.001$), a major interhemispheric pathway that connects limbic regions of the temporal lobe and prefrontal structures (*60*). These streamlines extended into fronto- and limbic-striatal circuits, including the inferior fronto-occipital fasciculus, inferior and middle longitudinal fasciculus, cingulum (temporal subsection), fornix, and arcuate fasciculus, as well as unilateral engagement of the left anterior thalamic radiation connecting the left thalamus, putamen, and NAcc (Fig. 4C). Additional bilateral engagement was observed in fibers of the forceps major, optic radiation, and acoustic radiation, all of which were associated with SIB improvement.

To study engagement of functional networks, we performed whole-brain seed-to-voxel functional connectivity analysis using each participant's VAT as the seed, mapped to a normative connectome [$n = 1000$; see Materials and Methods; (*61*, *62*)]. Whole-brain voxel-wise linear regression identified several sensorimotor, limbic,

Table 1. SIB and quality of life outcomes for participants undergoing NAcc-DBS. PedsQL, Pediatric Quality of Life Inventory; RBS-R, Repetitive Behavior Scale-Revised; SIB, self-injurious behavior.

Subject	RBS-R SIB score		RBS-R SIB percent change (%)	PedsQL total score		PedsQL total score percent change (%)
	Baseline	1-year follow-up		Baseline	1-year follow-up	
1	18	8	−55.6	4.3	18.5	325.0
2	11	3	−72.7	28.4	69.3	144.0
3	11	6	−45.5	48.5	52.2	7.51
4	13	14	7.7	21.7	16.3	−25.0
5	19	9	−52.6	10.0	45.7	356.5
6	17	9	−47.1	42.4	59.8	41.0

and striatal brain regions where connectivity strength correlated to reductions in RBS-R SIB subscores (Fig. 4D and fig. S4; $P_{permutate} < 0.01$). Greater improvement in SIB subscore was associated with weaker functional connectivity between the VAT and several motor and prefrontal regions, including the SMA, precentral gyrus (primary motor cortex), frontal, central, and parietal opercula, and PFC, including the inferior frontal gyrus and ACC. These regions are involved in motor control and have been previously linked to behavioral dysregulation in ASD (*20*, *63*). In parallel, SIB improvement was associated with stronger functional connectivity between the VAT and limbic regions—including the hippocampi, amygdalae, and insulae—as well as parietal and temporal regions (i.e., precuneus, angular gyrus, and middle, superior, and inferior temporal gyri) involved in memory and self-referential processing (*58*, *59*).

Longitudinal structural changes after NAcc-DBS in children with SIB

Last, we examined whether the network-level structural changes induced by NAcc-DBS in children with severe SIB were similar with those observed in the BTBR mouse using comparable deformation-based metrics. Using longitudinal T1-weighted MRI scans acquired at baseline and 1-year postimplantation, we applied DBM [see Materials and Methods; (*64*)] to assess NAcc-DBS–related brain volume changes. After 1 year of active NAcc-DBS, the participants exhibited significant volume reduction in regions linked to reward or emotional processing, including the caudate nucleus, putamen, ACC, and right hippocampus [Fig. 5; (*10*)]. These findings parallel the smaller striatum, parietotemporal cortex, and hippocampus volumes detected in BTBR mice subjected to NAcc electrical stimulation (Fig. 2). Conversely, volume increases were observed in areas involved in motor control (left primary motor cortex and cerebellar nuclei) (*65*, *66*), social-emotional processing (left temporal pole, left parahippocampal gyrus, and left insula) (*67*–*69*), and pain modulation (periaqueductal gray) (*70*). Larger volume was also detected within motor-related regions of the PFC in DBS-ON BTBR mice (Fig. 2). While several homologous structures were affected in both BTBR mice and children with severe SIB following NAcc stimulation, regional differences in the direction of volume change were observed in the PFC, SMA, and habenula (Fig. 5, B and C). Furthermore, species-specific effects were observed, with BTBR mice showing significant volume change in the primary and secondary somatosensory area (S1/S2) and amygdala, whereas human participants exhibited significant changes in the insula that were not observed in the mouse cohort. Nevertheless, these cross-species findings reveal a shared pattern of structural plasticity induced by NAcc-targeted stimulation, extending beyond the striatum to encompass distributed regions involved in reward and emotional processing, sensorimotor integration, and pain modulation. In both mice and humans, volume differences were detected along homologous sensorimotor, limbic, and striatal structures, supporting the existence of a conserved fronto-limbic-striatal network involved in regulation of pathological SIB and responsive to NAcc stimulation.

DISCUSSION

We demonstrate that targeted stimulation of the NAcc can influence corticostriatal circuitry implicated in the expression of SIB in ASD, as evidenced by a mouse model and data from a first-in-human clinical trial. Given that restricted and repetitive behaviors in ASD carry a high risk of severe physical harm, permanent disability, and death (*5*, *6*), elucidating the underlying neural circuitry is crucial to develop effective, circuit-informed interventions. We leveraged a cross-species framework and show that targeted electrical stimulation of the NAcc modulates corticostriatal circuitry, leading to reductions in SIB through structural and functional alterations of a conserved fronto-limbic-striatal network.

Findings from the human clinical trial demonstrate that NAcc-DBS appears safe and feasible for children with profound ASD and severe, treatment-refractory SIB, with evidence of early clinical efficacy (*46*). Consistent with these clinical findings, we demonstrate that in the translational BTBR mouse model, targeted NAcc electrical stimulation selectively reduces both SIB and repetitive behavior relative to unstimulated controls. BTBR mice begin to exhibit injurious self-grooming during the juvenile period, and this repetitive behavior persists throughout the lifespan (*49*). As a result, the associated physical injuries typically worsen over time in the absence of effective interventions to mitigate the repetitive and excessive levels of self-grooming. Here, reductions in visible self-inflicted injuries after NAcc stimulation appeared to result not only from the relative stability of self-grooming duration but also from improved grooming sequence organization, as shown by a significantly lower proportion of incorrect transitions in the cephalocaudal pattern (*48*, *50*). This trend parallels clinical observations, where individuals may engage in SIB for similar durations, yet differences in the type and severity of behaviors can result in varying levels of physical injury (*71*, *72*). Experimental lesions to the striatum and ventral pallidum

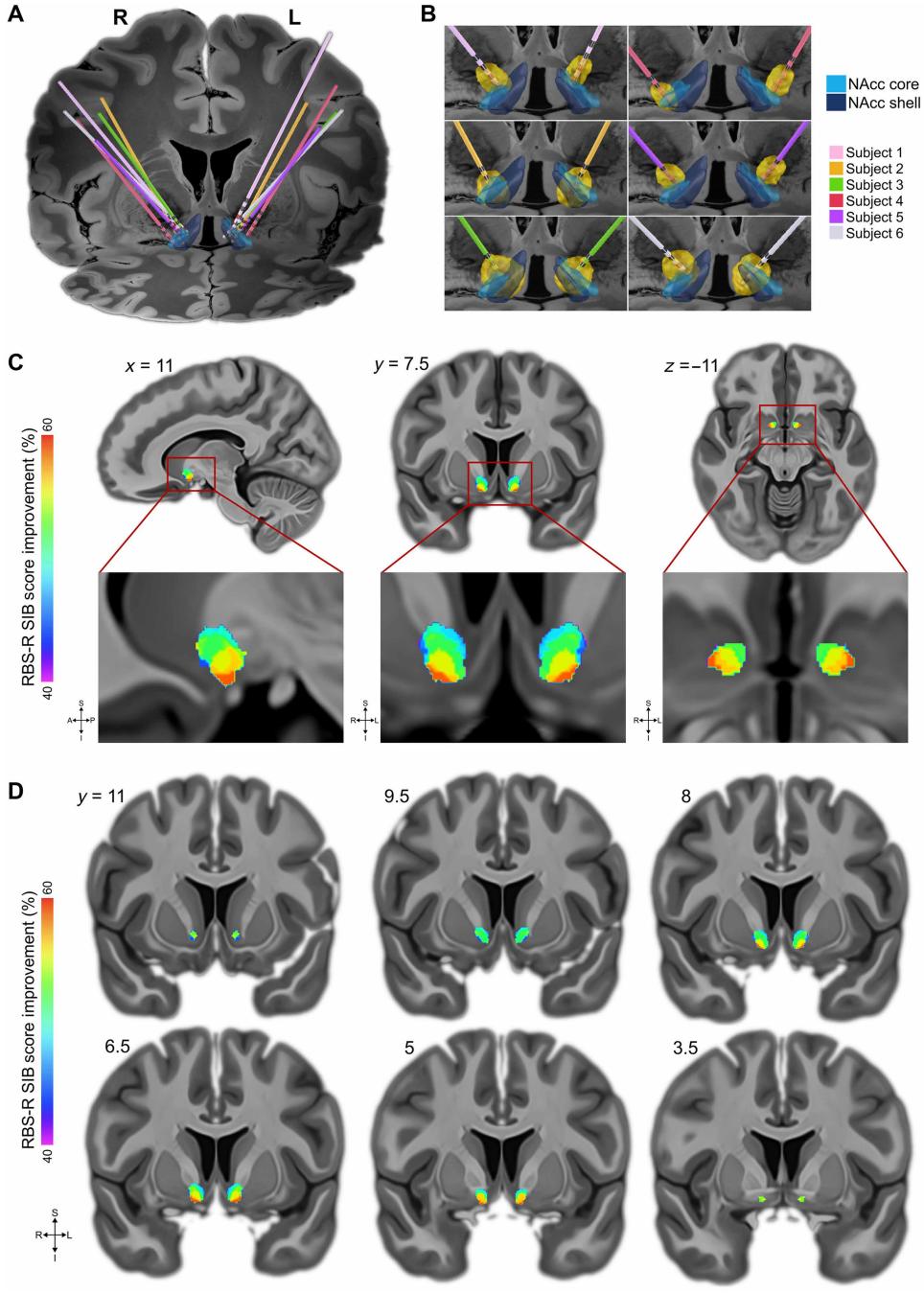

Fig. 3. NAcc-DBS sweet-spot mapping in participants with SIB and ASD. (**A**) Electrode placement shown in relation to the NAcc core (light blue) and shell (dark blue; $n = 6$). Subject 4 presented with multiple baseline brain abnormalities, leading to the left DBS electrode appearing to be lateral to the NAcc in this standard-space template. Anatomical review of individual postoperative MRI confirmed accurate placement within the targeted region. (**B**) Bilateral VAT (yellow) of each subject calculated from the stimulation parameters (table S4) applied after 1-year of active NAcc-DBS. Active contacts are colored in red. (**C**) Probabilistic map showing the voxels that are significantly ($P < 0.05$) associated with greater SIB improvement (red), measured by the RBS-R (*57*). The probabilistic map was thresholded using a Wilcoxon signed-rank test ($P < 0.05$, at each voxel), followed by nonparametric permutation testing ($P_{permute} < 0.001$). (**D**) The extent of the VATs responsible for eliciting at least 40% improvement is shown in successive coronal slices. NAcc, nucleus accumbens.

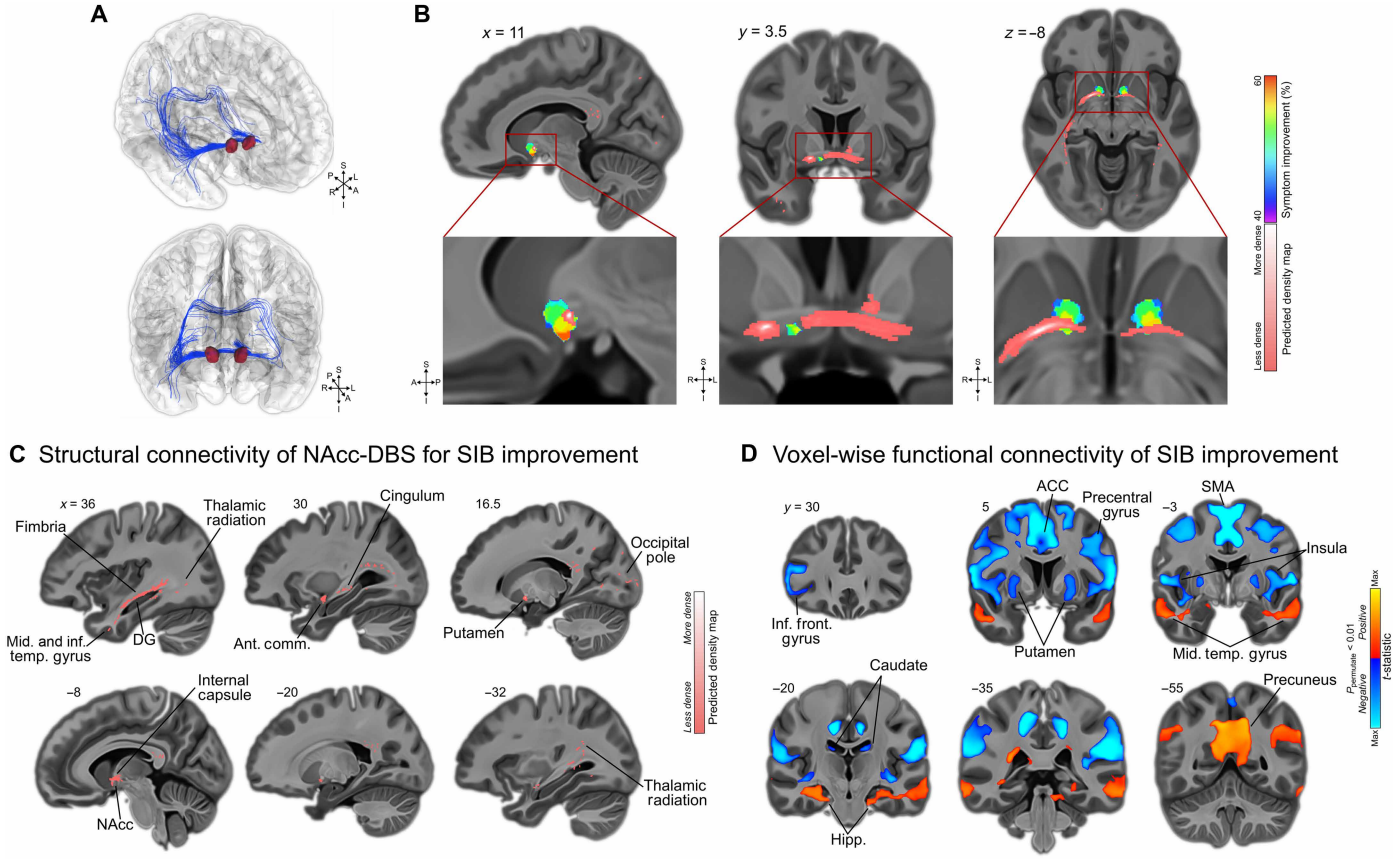

Fig. 4. Structural and functional connectivity of NAcc-DBS for improving SIB in participants with ASD. (**A**) Streamlines associated with greater SIB improvement, illustrated on the MNI152 brain. Blue, streamlines; red, VAT. (**B**) MRI showing the relation between VATs responsible for eliciting at least 40% SIB improvement and the fiber density map. (**C**) Streamlines connected to the VATs associated with significantly greater SIB improvement. (**D**) Warm colors (positive) indicate regions where stronger functional connectivity with the VAT is associated with greater SIB improvement, while cool colors (negative) indicate regions where weaker functional connectivity with the VAT is associated with greater SIB improvement. ACC, anterior cingulate cortex; DG, dentate gyrus; Front., frontal; Hipp., hippocampus; Inf., inferior; Mid., middle; NAcc, nucleus accumbens; SMA., supplementary motor area; Temp., temporal.

disrupt grooming syntax and prolong grooming bouts, emphasizing the role of these regions in the temporal and spatial structuring of innate motor sequences (*31*–*33*).

Structurally, BTBR mice exhibit enlarged striatal volume relative to non-ASD strains—a characteristic strongly associated with heightened self-grooming and stereotyped behaviors (*73*). Our DBM analysis revealed that NAcc stimulation resulted in smaller striatum and pallidum volumes in DBS-ON mice compared to unstimulated controls. These volumetric differences correlated with decreased injurious self-grooming and repetitive marble-burying, suggesting that NAcc-targeted modulation can reduce atypical striatal morphology and, in turn, restore inhibitory control over maladaptive motor patterns.

Similarly, neuroimaging studies in humans with ASD have linked increased striatal volume to greater severity of restricted and repetitive behaviors (*28*, *74*). Accordingly, our clinical cohort showed significant longitudinal reductions in striatal volume alongside clinical improvement, further supporting the notion that NAcc stimulation may reduce SIB through normalization of striatum morphology. Extending these findings, we found that chronic NAcc stimulation induced structural and functional alterations within homologous cortical and limbic regions in both BTBR mice and humans, which were associated with clinical reductions of SIB. These observations align with prior neuroimaging studies in ASD, which have consistently implicated dysregulated corticostriatal and limbic networks in the pathophysiology of repetitive behaviors (*20*–*23*, *28*).

The current findings also intersect with broader models of motivation and reward circuitry. Converging evidence from animal and human studies have implicated a central role of the NAcc in cortico-limbic regulation of motivational drive and reinforcement learning—processes that are tightly involved in the expression of repetitive and impulsive behaviors (*75*–*77*). Motivation, reward, and habit-related behaviors rely on overlapping corticostriatal and limbic networks (*77*) such that modulation of NAcc activity can influence the balance between goal-directed and stereotyped responding. Optogenetic studies demonstrate that dopaminergic input from the ventral tegmental area to the NAcc produces a generic motivation signal capable of reinforcing even spontaneous actions (*78*–*80*). Thus, reductions in SIB and repetitive behavior following NAcc-DBS may reflect a recalibration of motivational drive that disrupts reinforcement of pathological motor sequences. However, the absence of changes in exploratory behavior or social interactions suggests that

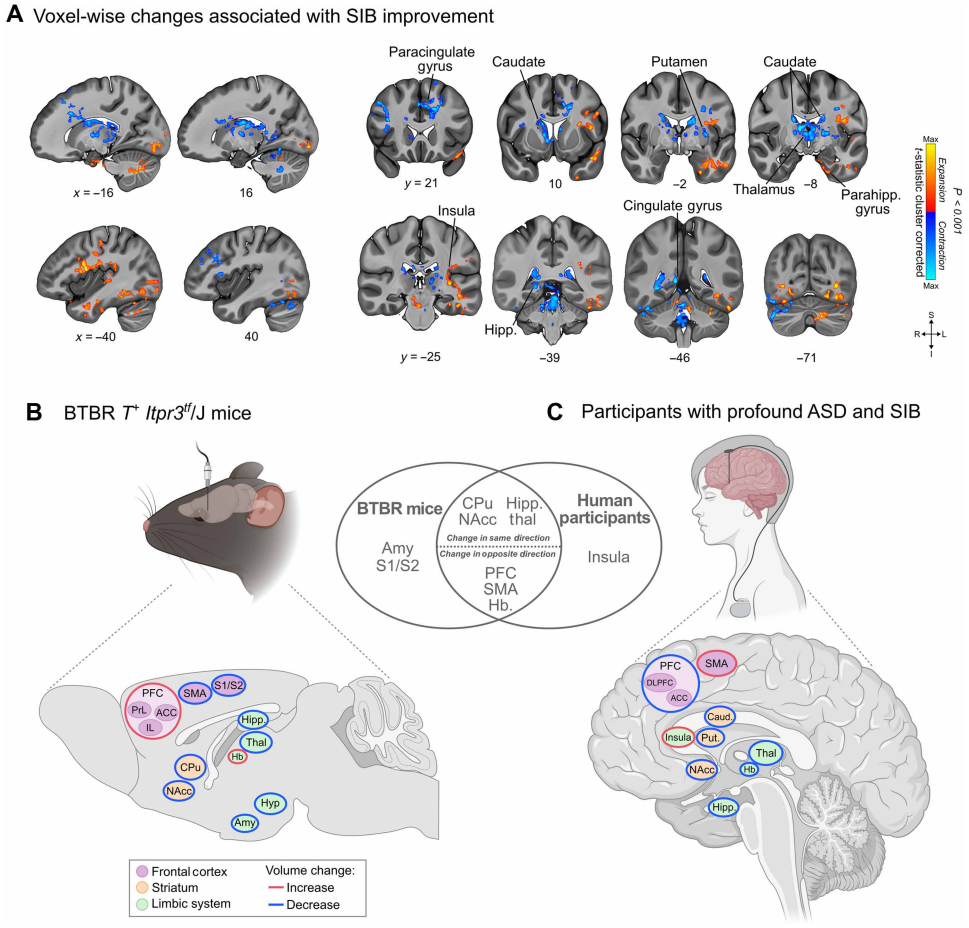

Fig. 5. Volume changes after NAcc-DBS in participants with profound ASD and SIB and BTBR mice. (**A**) Longitudinal DBM of children treated with NAcc-DBS for 1 year. Significant voxel-wise volume increase (warm colors) and decrease (cold colors) associated with RBS-R SIB subscore improvement at 1-year follow-up. Summary of volume changes along the fronto-limbic-striatal network of (**B**) BTBR mice and (**C**) clinical trial participants after NAcc-DBS. Created in BioRender. Zhang, K. (2025) https://BioRender.com/bou28l2. Structures exhibiting overall volume increase and decrease are outlined in red and blue, respectively. Venn diagram lists the fronto-limbic-striatal structures demonstrating significant volume change and concordance of change direction across species. ACC, anterior cingulate cortex; Amy, amygdala; Caud., caudate nucleus; CPu, caudoputamen; DLPFC, dorsolateral prefrontal cortex; GP, globus pallidus; Hb, habenula; Hipp., hippocampus; Hyp, hypothalamus; IL, infralimbic cortex, SMA, supplementary motor area; NAcc, nucleus accumbens; PFC, prefrontal cortex; PrL, prelimbic cortex; Put., putamen; S1/S2, primary and secondary somatosensory area; Thal, thalamus.

these effects are unlikely to stem from a general reduction in motivation but rather point toward selective modulation of circuits linking reinforcement learning to repetitive and self-injurious actions.

Reinforcing signals within frontostriatal circuits involving the NAcc are thought to contribute to the automatic maintenance of repetitive behaviors, including SIB (*13*). NAcc-DBS has shown promise in normalizing frontostriatal dynamics (*81*) and reducing the severity (*82*, *83*) of obsessive-compulsive disorder (OCD)—a condition also characterized by impaired inhibitory control (*17*). Here, we identified volumetric differences in frontal cortices of BTBR mice and humans after NAcc-DBS, along with reduced functional connectivity with the ACC, primary motor cortex, and SMA. These findings are concordant with the results of a functional MRI study in OCD, where baseline hyperconnectivity between the NAcc and dorsomedial PFC was normalized following NAcc-DBS, with the extent of connectivity reduction correlating with symptom improvement (*83*). Similarly, stronger connectivity between the striatum and ACC has been reported in ASD (*20*). While the literature remains mixed regarding which specific frontostriatal circuits are disrupted—and whether they manifest as hyper- or hypoconnectivity—there is converging evidence that an imbalance within frontostriatal and thalamo-cortical networks underlies the deficits in inhibitory control observed in ASD and SIB (*84*).

Structural connectivity and brain organization are known to shape functional connectivity (*85*). Thus, our multimodal framework incorporating whole-brain structural and functional connectivity analyses with DBM to identify widespread structural abnormalities enables a comprehensive characterization of the basal ganglia-thalamo-cortical regions involved in restoring patterns of inhibitory control. Habit formation and behavioral control are also intricately regulated by limbic-striatal circuits involving the NAcc (*7*, *13*, *21*). Our functional connectivity analysis revealed that greater SIB reduction was linked to stronger connectivity between the NAcc stimulation site and limbic and associative areas, including the hippocampi, amygdalae, temporal gyri, and precuneus. While limbic-striatal hyperconnectivity is frequently reported in individuals with ASD and

elevated repetitive behaviors (*20*, *21*), our findings suggest that the therapeutic effects of NAcc-DBS may not simply arise from reversing this elevated functional connectivity. Instead, the posttreatment increases observed here may reflect a shift from disorganized, maladaptive signaling to more coherent and functionally integrated network engagement. Strengthened connectivity could represent enhanced fidelity and coordination of limbic inputs within striatal circuits, facilitating more adaptive modulation of emotional salience and behavioral output. These findings point to a neuromodulatory mechanism wherein NAcc-DBS facilitates adaptive engagement of limbic-striatal networks involved in behavioral regulation, rather than merely suppressing circuit overactivity.

These functional changes were paralleled by structural alterations within limbic-striatal regions. Prior studies have reported enlarged hippocampal volume in both patients with ASD and BTBR mice, correlating with high levels of repetitive behaviors (*73*, *86*). Abnormal thalamic volume has also been consistently reported in ASD, although the direction of these differences remains inconsistent across studies (*87*, *88*). Our DBM analyses revealed a cross-species normalization pattern, with significantly smaller hippocampal and thalamic volumes following chronic NAcc stimulation in both mice and humans, suggesting a convergent structural response within the limbic-striatal network. These volumetric differences were not limited to individual regions but rather reflect broader modulation of a network of interconnected subcortical and cortical limbic structures that interface with the striatum, contributing to behavioral flexibility, affect regulation, and motor control (*10*, *11*).

The robust volumetric changes observed in BTBR mice are consistent with previous reports demonstrating that both acute and chronic stimulation paradigms can induce measurable structural plasticity in rodents (*89*, *90*). Such neuroplastic adaptations are thought to arise from activity-dependent processes, including alterations in dendritic spine density, synaptic remodeling, neurovascular reorganization, glial dynamics, and epigenetic modifications (*90*–*94*). Experimental rodent studies have shown that NAcc stimulation inhibits neuronal activity in the ventral pallidum and ventral tegmental area (*95*, *96*), shifts excitatory/inhibitory balance locally and across connected networks (*95*, *97*), enhances hippocampal activity and neurogenesis (*98*, *99*), and increases monoamine transmission in frontal cortical regions (*100*). While the precise cellular mechanisms underlying NAcc-DBS for SIB and repetitive behaviors remain to be fully delineated, our results indicate that DBS-evoked volumetric changes reflect biologically meaningful neuroplastic adaptations with functional relevance for network organization. The convergence of structural changes among BTBR mice and humans with SIB undergoing NAcc-DBS strengthens the translational value of these findings and suggests that comparable cellular processes may underlie the network-level effects observed across species.

NAcc-DBS in our human cohort also engaged the anterior thalamic radiation linking the NAcc stimulation site to the putamen and left thalamus. These tracts carry reciprocal connections between thalamic nuclei and the PFC, supporting inhibitory control and modulating reinforcement of repetitive and impulsive behavior (*101*). Moreover, we found a high density of fiber tracts traversing the anterior commissure, projecting toward midline and posterior cortical regions. These tracts support interhemispheric integration of sensory information (*60*), particularly within temporal limbic structures, which, in our study, also demonstrated volumetric alterations and functional engagement. Given the anterior commissure's known role in coordinating bilateral limbic processing, these connections may contribute to the normalization of dysregulated sensory-affective signaling following NAcc-DBS.

Building on prior evidence linking NAcc activation to salience processing of both emotional and sensory stimuli (*102*, *103*), we observed structural engagement in sensory-processing limbic regions and fiber pathways mediating sensory-affective signaling. This offers insight into the involvement of limbic-striatal circuits on the neural basis of sensory integration in ASD. In previous work, we also reported longitudinal [^{18}F]fluorodeoxyglucose positron emission tomography (PET) results demonstrating stimulation-induced reductions in metabolic activity within the dorsal striatum, thalamus, insula, and temporal cortices (*46*). Combining the functional and structural circuit effects observed here with the PET findings, we suggest that NAcc-DBS exerts network-level effects across limbic-striatal and sensory integration circuits. By enhancing the coordination between these systems, NAcc-DBS may help restore balance between excitatory limbic inputs and reducing SIB.

In addition to the clinical trial we present, prior case reports have attempted to stimulate a range of subcortical targets to mitigate extreme behaviors in ASD, including the basolateral amygdala (*41*), globus pallidus (*42*), and posterior hypothalamus (*43*). A recent connectomic meta-analysis showed that stimulation of disparate targets may converge on a common limbic-striatal network anchored by the ventral capsule and ventral striatum (*44*), which involves the NAcc. Our findings advance this understanding by moving beyond correlative evidence and demonstrating a direct causal relationship between NAcc stimulation and circuit-level changes associated with SIB improvement. Given the robust impact of stimulation site on clinical outcomes, identifying the NAcc subregion associated with greatest group-level symptom improvement is essential for symptom-specific targeting and parameter optimization in these clinically heterogeneous populations.

In our human cohort, voxel-efficacy mapping revealed a distinct gradient, indicating that SIB reduction was associated with a stimulation sweet-spot in the inferior and lateral part of the NAcc—corresponding to the NAcc core, which is recognized for its pivotal role in regulating goal-directed behaviors (*104*, *105*). This region forms extensive projections to motor-related structures such as the dorsal striatum and thalamus (*14*), which we observed to undergo morphological changes following NAcc-DBS. This study identifies an optimal stimulation site within the NAcc for treating SIB in the specific context of ASD. Relevance in other contexts will need to be considered carefully. While tractography studies in OCD suggest that dorsoventral stimulation may yield more favorable clinical outcomes (*106*), others found that dorsal NAcc stimulation may worsen impulsivity (*107*), underscoring the importance of symptom-specific targeting and parameter optimization in these heterogeneous populations.

Some studies indicate that high-frequency stimulation may exert therapeutic effects by increasing neuronal activity within the stimulated nucleus (*108*, *109*). In contrast, other results suggest that high-frequency stimulation produces inhibition through depolarization block or activation of inhibitory neurons (*110*–*112*). In rodent models of compulsivity, NAcc-DBS has been shown to reduce local neural firing rates and glutamate levels, thereby suppressing hyperactive and aberrant excitability (*113*). Other studies in compulsivity models have reported both excitatory and inhibitory responses associated with behavioral improvements following DBS (*114*). Furthermore,

DBS is thought to preferentially stimulate axon terminals and axons of passage relative to cell bodies (*115*, *116*), which results in broader, circuit-level influences (*117*, *118*). In line with this framework, our structural neuroimaging and connectivity analyses demonstrate that NAcc-DBS produces a robust network-level impact. These findings suggest that, even if local inhibitory processes occur within the NAcc, their downstream effects manifest at the circuit level, leading to widespread reorganization of network interactions. Thus, our study provides valuable insight into the regions and pathways through which DBS exerts therapeutic benefit in SIB and forms the basis to which future studies, using neurotransmitter assays and in vivo electrophysiology, can directly assess the role of local inhibitory mechanisms in the context of NAcc-DBS for SIB.

Despite the strengths of cross-species work and a first-in-human clinical trial, our study has several limitations. Not all anatomical-behavioral correlations in BTBR mice survived the more conservative correction threshold ($q_{FDR} < 0.05$); however, several fronto-limbic-striatal regions showed strong associations that were significant after FDR correction. Given their alignment with prior literature and known network-level involvement in emotional reactivity and behavioral inhibition, these correlations are likely to provide meaningful insights for understanding the circuit mechanisms of repetitive and SIBs. The patient data come from a small, albeit uniquely valuable, cohort of six children in a phase 1 pilot trial. While these findings provide important insights, the small sample size constrains the generalizability of both the clinical outcomes and DBS mapping analyses. Given that SIB can arise from diverse etiologies and present with varying forms and degrees of severity, larger studies are needed to validate and expand on the foundational findings presented here. On the basis of promising results of the phase 1 human study, together with mechanistic insights from the BTBR mouse, an ongoing double-blinded randomized clinical trial is currently seeking to better characterize the efficacy of NAcc-DBS in children with severe, refractory SIB (ClinicalTrials.gov, NCT06529380). We also used normative connectomes for connectivity analyses, which, while offering high resolution and reduced noise, may not fully capture developmental and disease-specific differences. Still, key connectivity pathways are largely conserved across ages (*119*), supporting their relevance. Normative datasets offer superior data quality, largely because of longer scan durations and fewer motion artifacts compared to clinical populations such as individuals with SIB or ASD. To refine our foundational findings presented here, future preclinical studies should aim to systematically manipulate specific regions and white matter tracts to better link stimulation targets with behavioral and network dynamics.

Together, our findings advance mechanistic insight into the neural circuitry underlying SIB and delineate how targeted modulation of corticostriatal networks can drive SIB improvement in ASD. We demonstrate that electrical stimulation of the NAcc not only reduces SIB but also induces structural remodeling across limbic, striatal, somatosensory, and motor regions, highlighting its distributed network effects. In children, connectomic analyses identified engagement of fronto-limbic-striatal circuits as a key substrate of therapeutic response. These findings provide a critical mechanistic framework for understanding how circuit-level plasticity underlies behavioral change and establishes a foundation for future studies aimed at refining corticostriatal neuromodulation to optimize outcomes in an extremely vulnerable population of children with SIB.

MATERIALS AND METHODS

Experimental design

This study aimed to investigate the effects of targeted NAcc electrical stimulation on corticostriatal networks and maintenance of SIB in ASD. For preclinical studies, BTBR mice (10 weeks old, male) were randomly assigned to DBS-ON, DBS-OFF, or Control groups. DBS-ON and DBS-OFF mice received bilateral NAcc electrode implants and an anchoring screw. Control mice received only the anchoring screw to control for anesthesia effects and surgical procedures. After postoperative recovery, all animals were evaluated for ASD-relevant behaviors: injurious self-grooming (*49*), repetitive behavior [marble-burying; (*120*)], anxiety-like behavior and locomotor activity [open field; (*121*)], and social interaction [three-chamber social approach; (*122*)]. All animals were housed in DVC cages, which maintain standard housing conditions while enabling continuous monitoring of spontaneous circadian and locomotor activity. Following baseline behavior testing, DBS-ON mice received active NAcc stimulation for four consecutive days (5 hours/day; 100 μA, 100 Hz, 60 μs; biphasic mode), while DBS-OFF mice were connected to the stimulator without active stimulation, and Control mice were not connected but kept in the same room, with matched conditions. After the stimulation period, BTBR mice were reassessed for the same behaviors as at baseline. Subsequently, the brains were perfusion fixed (*123*) for T2-weighted MRI, followed by DBM (*54*) to evaluate volume differences across brain regions between groups. All procedures were approved by the Animal Care Committee of The Centre for Phenogenomics (Animal Use Protocol: 29-0355H) and complied with Canadian Council on Animal Care guidelines and the Animals for Research Act of Ontario. This study followed the Animal Research: Reporting of In Vivo Experiments guidelines (*124*).

For investigation in humans, we leveraged data from participants enrolled in a first-in-human trial of NAcc-DBS for severe, treatment-refractory SIB. This phase 1 clinical trial was approved by the Hospital for Sick Children's Research Ethics Board (1000060282PID) and monitored by Health Canada. The trial protocol was registered in ClinicalTrials.gov (NCT03982888) and previously published (*125*).

To investigate the relationship between stimulation location and treatment response, bilateral electrode placements were localized, and VATs were modeled for each participant (*58*). To identify the stimulation sweet-spot related with greater SIB improvement, probabilistic efficacy mapping (*126*) was performed using RBS-R SIB subscores from baseline and 1-year follow-up. VATs were further processed for connectomic analyses (*61*, *62*) to investigate the structural (i.e., fiber tracts) and functional (i.e., brain areas) maps associated with SIB improvement among children treated with NAcc-DBS. To examine network-level structural changes induced by NAcc-DBS, we applied DBM (*64*) to longitudinal T1-weighted MRIs collected at baseline and 1-year postimplantation. Details regarding behavior testing and imaging protocols used in the preclinical arm, as well as processing parameters and statistical approaches in the clinical imaging analysis, are included in the Supplementary Materials.

Statistical analyses

Mouse behavior testing

Mouse behavior was analyzed in R (v4.4.1) using the lme4 (v1.1-35.5) package. The variables analyzed are described in table S1. Linear regression compared self-grooming metric and bald area between groups. Linear mixed-effects models analyzed marble burying, open field behavior, three-chamber social approach outcomes,

and home-cage activity across groups and test sessions. Circadian activity rhythms were analyzed using the GLMMcosinor package (v0.2.1) in R. The level of significance was set at $P < 0.05$.

Mouse brain volume and behavior correlations

Voxel-wise cluster volumes were segmented into 62 different regions according to the Dorr-Steadman-Ullman-Richards-Qiu-Egan 40-μm atlas (*55*). Pearson correlations were performed between 62 different regional volumes and four behavioral metrics (absolute volume versus self-grooming time, proportion of correct grooming transitions, proportion of physically injured body area, and number of marbles buried) after treatment. This allowed the comparison of brain volume differences to behavior outcomes across treatment groups. Significant correlations were corrected for multiple comparisons with FDR.

Deformation-based morphometry

Structural MRI of BTBR mice were postprocessed for geometric distortions and analyzed using DBM, as previously described (*54*). Briefly, images were linearly (6 parameters followed by 12 parameters) and nonlinearly registered together with mni_autoreg (*127*) and Advanced Normalization Tools [ANTS; (*128*, *129*)]. Jacobian determinants of the deformation field were calculated as measures of volume at each voxel. Multiple test correction was applied across all the voxels in the whole-brain mask based on family-wise error rate, which was performed with a cluster-based statistical method implemented in the Analysis of Functional NeuroImages (AFNI) 3dClustSim software suite (*130*). Cluster significance thresholds were derived from Monte Carlo simulations with 10,000 iterations (*131*). Given the size of the whole brain mask, the minimum cluster extent was 1882 voxels (121 mm^3) to reach $P < 0.05$ at the voxel level and $P < 0.001$ at the cluster level.

For human data, longitudinal DBM was implemented as previously described (*64*). Briefly, images were linearly and nonlinearly registered using ANTS in a two-level registration procedure: (i) Images of the same subject were registered to an iteratively updated average to detect within subject changes occurring over time, and (ii) subject averages were registered to an iteratively updated population average to achieve voxel correspondence to compare the local individual changes across the group of subjects. Log-transformed Jacobians were smoothed using a 2-mm 3D Gaussian kernel. Voxel-wise statistical modeling was performed using RMINC (v1.5.2.2) mixed-effect linear models, with a fixed effect of (pseudo) time point and a random intercept by subject. Multiple comparisons were corrected using the aforementioned AFNI 3dClustSim program (*130*). On the basis of Monte Carlo simulations, a voxel-wise threshold was applied, and a minimum cluster size of 17,569 voxels (2197 mm^3) was required to maintain significance at $P < 0.05$ at the voxel level and $P < 0.001$ at the cluster level.

Probabilistic efficacy mapping

Lead-DBS software (https://lead-dbs.org/) was used for electrode localization and modeling of each individual's VAT, as previously described (*58*). Each VAT was assigned its corresponding percentage of improvement after 1-year of treatment. Mean improvement of overlapping VATs was calculated at each voxel. The resulting average map was then thresholded for voxel-wise significance using a Wilcoxon signed-rank test ($P < 0.05$). For each voxel, the Wilcoxon-signed rank test compared clinical improvement between participants whose VAT overlapped the voxel and those whose VAT did not. This approach denoted whether stimulation was associated with a significant clinical improvement at each voxel. The validity of the voxel efficacy map was determined through nonparametric permutation testing ($P_{permute} < 0.001$), in which each clinical outcome score was randomly assigned to a random VAT.

Imaging connectomics

To identify white matter pathways associated with positive treatment outcome, we first extracted all streamlines intersecting each participants' VAT (i.e., seed region) from a normative whole-brain tractography template comprising ~12 million streamlines (*59*). To determine the streamlines significantly associated with positive treatment outcome, a *t* test of symptom improvement comparing subjects whose VAT touched a given streamline and individuals who did not was performed, as previously described (*62*). The results were corrected for multiple comparisons using FDR at $q_{FDRcor} < 0.001$.

To evaluate functional connectivity, a whole-brain correlation map (r-map) was computed for each subject's bilateral VATs based on the resting-state functional MRI blood-oxygen level dependent time course-dependent correlations between the seed regions and remaining voxels across a normative connectome (*59*). Whole-brain voxel-wise linear regression was performed to test the relationship between magnitude of functional correlation and symptom improvement. Threshold free cluster enhancement was applied to the functional connectivity map with subsequent permutation testing, resulting in a statistical map corrected for multiple testing, thresholded at $P < 0.01$.

Supplementary Materials

The PDF file includes:

Supplementary Materials and Methods
Figs. S1 to S5
Tables S1 to S4
Legends for data S1 and S2
References

Other Supplementary Material for this manuscript includes the following:

Data S1 and S2

REFERENCES

1. K. Zhang, G. M. Ibrahim, F. Venetucci Gouveia, Molecular pathways, neural circuits and emerging therapies for self-injurious behaviour. *Int. J. Mol. Sci.* **26**, 1938 (2025).
2. B. J. Wilkes, D. B. Archer, A. L. Farmer, C. Bass, H. Korah, D. E. Vaillancourt, M. H. Lewis, Cortico-basal ganglia white matter microstructure is linked to restricted repetitive behavior in autism spectrum disorder. *Mol. Autism.* **15**, 6 (2024).
3. L. A. Shawler, J. L. Becraft, L. P. Hagopian, "Self-injurious behavior" in *Handbook of Clinical Child Psychology* (Springer International Publishing, 2023), pp. 811–828.
4. L. P. Hagopian, G. W. Rooker, J. R. Zarcone, Delineating subtypes of self-injurious behavior maintained by automatic reinforcement. *J. Appl. Behav. Anal.* **48**, 523–543 (2015).
5. V. Totsika, S. Toogood, R. P. Hastings, S. Lewis, Persistence of challenging behaviours in adults with intellectual disability over a period of 11 years. *J. Intellect. Disabil. Res.* **52**, 446–457 (2008).
6. V. Bradley, D. Hiersteiner, D. Rotholz, J. Maloney, H. Li, A. Bonardi, J. Bershadsky, Personal characteristics and outcomes of individuals with developmental disabilities who need support for self-injurious behaviour. *J. Intellect. Disabil. Res.* **62**, 1043–1057 (2018).
7. C. L. Burton, A. Longaretti, A. Zlatanovic, G. M. Gomes, R. Tonini, Striatal insights: A cellular and molecular perspective on repetitive behaviors in pathology. *Front. Cell. Neurosci.* **18**, 1386715 (2024).
8. S. N. Haber, J. L. Fudge, N. R. McFarland, Striatonigrostriatal pathways in primates form an ascending spiral from the shell to the dorsolateral striatum. *J. Neurosci.* **20**, 2369–2382 (2000).
9. B. W. Balleine, J. P. O'Doherty, Human and rodent homologies in action control: Corticostriatal determinants of goal-directed and habitual action. *Neuropsychopharmacology* **35**, 48–69 (2010).
10. S. N. Haber, Corticostriatal circuitry. *Dialogues Clin. Neurosci.* **18**, 7–21 (2016).
11. G. E. Alexander, M. R. DeLong, P. L. Strick, Parallel organization of functionally segregated circuits linking basal ganglia and cortex. *Annu. Rev. Neurosci.* **9**, 357–381 (1986).
12. J. H. Balsters, D. Mantini, N. Wenderoth, Connectivity-based parcellation reveals distinct cortico-striatal connectivity fingerprints in autism spectrum disorder. *Neuroimage* **170**, 412–423 (2018).

13. G. Kohls, B. E. Yerys, R. T. Schultz, Striatal development in autism: Repetitive behaviors and the reward circuitry. *Biol. Psychiatry* **76**, 358–359 (2014).
14. H. Yan, N. A. Shlobin, Y. Jung, K. K. Zhang, N. Warsi, A. V. Kulkarni, G. M. Ibrahim, Nucleus accumbens: A systematic review of neural circuitry and clinical studies in healthy and pathological states. *J. Neurosurg.* **138**, 337–346 (2023).
15. J. M. Welch, J. Lu, R. M. Rodriguiz, N. C. Trotta, J. Peca, J.-D. Ding, C. Feliciano, M. Chen, J. P. Adams, J. Luo, S. M. Dudek, R. J. Weinberg, N. Calakos, W. C. Wetsel, G. Feng, Cortico-striatal synaptic defects and OCD-like behaviours in Sapap3-mutant mice. *Nature* **448**, 894–900 (2007).
16. J. Peça, C. Feliciano, J. T. Ting, W. Wang, M. F. Wells, T. N. Venkatraman, C. D. Lascola, Z. Fu, G. Feng, Shank3 mutant mice display autistic-like behaviours and striatal dysfunction. *Nature* **472**, 437–442 (2011).
17. C. Burbidge, C. Oliver, J. Moss, K. Arron, K. Berg, F. Furniss, L. Hill, K. Trusler, K. Woodcock, The association between repetitive behaviours, impulsivity and hyperactivity in people with intellectual disability. *J. Intellect. Disabil. Res.* **54**, 1078–1092 (2010).
18. C. Richards, L. Davies, C. Oliver, Predictors of self-injurious behavior and self-restraint in autism spectrum disorder: Towards a hypothesis of impaired behavioral control. *J. Autism Dev. Disord.* **47**, 701–713 (2017).
19. L. E. Davies, C. Oliver, Self-injury, aggression and destruction in children with severe intellectual disability: Incidence, persistence and novel, predictive behavioural risk markers. *Res. Dev. Disabil.* **49–50**, 291–301 (2016).
20. S. Delmonte, L. Gallagher, E. O'Hanlon, J. McGrath, J. H. Balsters, Functional and structural connectivity of frontostriatal circuitry in autism spectrum disorder. *Front. Hum. Neurosci.* **7**, 430 (2013).
21. A. E. Abbott, A. C. Linke, A. Nair, A. Jahedi, L. A. Alba, C. L. Keown, I. Fishman, R.-A. Müller, Repetitive behaviors in autism are linked to imbalance of corticostriatal connectivity: A functional connectivity MRI study. *Soc. Cogn. Affect. Neurosci.* **13**, 32–42 (2018).
22. F. Augustine, M. B. Nebel, S. H. Mostofsky, E. M. Mahone, H. S. Singer, Aberrant prefrontal cortical-striatal functional connectivity in children with primary complex motor stereotypies. *Cortex* **142**, 272–282 (2021).
23. K. N. Thakkar, F. E. Polli, R. M. Joseph, D. S. Tuch, N. Hadjikhani, J. J. S. Barton, D. S. Manoach, Response monitoring, repetitive behaviour and anterior cingulate abnormalities in autism spectrum disorders (ASD). *Brain* **131**, 2464–2478 (2008).
24. M. Langen, A. Leemans, P. Johnston, C. Ecker, E. Daly, C. M. Murphy, F. Dell'acqua, S. Durston, AIMS Consortium, D. G. M. Murphy, Fronto-striatal circuitry and inhibitory control in autism: Findings from diffusion tensor imaging tractography. *Cortex* **48**, 183–193 (2012).
25. V. L. Corbit, E. E. Manning, A. H. Gittis, S. E. Ahmari, Strengthened inputs from secondary motor cortex to striatum in a mouse model of compulsive behavior. *J. Neurosci.* **39**, 2965–2975 (2019).
26. G. J. Gage, C. R. Stoetzner, A. B. Wiltschko, J. D. Berke, Selective activation of striatal fast-spiking interneurons during choice execution. *Neuron* **67**, 466–479 (2010).
27. M. D. Bauman, J. E. Toscano, B. A. Babineau, W. A. Mason, D. G. Amaral, Emergence of stereotypies in juvenile monkeys (Macaca mulatta) with neonatal amygdala or hippocampus lesions. *Behav. Neurosci.* **122**, 1005–1015 (2008).
28. M. Langen, D. Bos, S. D. S. Noordermeer, H. Nederveen, H. van Engeland, S. Durston, Changes in the development of striatum are involved in repetitive behavior in autism. *Biol. Psychiatry* **76**, 405–411 (2014).
29. J. Bachevalier, K. A. Loveland, The orbitofrontal-amygdala circuit and self-regulation of social-emotional behavior in autism. *Neurosci. Biobehav. Rev.* **30**, 97–117 (2006).
30. A. M. Graybiel, S. L. Rauch, Toward a neurobiology of obsessive-compulsive disorder. *Neuron* **28**, 343–347 (2000).
31. R. N. Cardinal, N. J. Howes, Effects of lesions of the nucleus accumbens core on choice between small certain rewards and large uncertain rewards in rats. *BMC Neurosci.* **6**, 37 (2005).
32. R. N. Cardinal, D. R. Pennicott, C. L. Sugathapala, T. W. Robbins, B. J. Everitt, Impulsive choice induced in rats by lesions of the nucleus accumbens core. *Science* **292**, 2499–2501 (2001).
33. G. Bezzina, T. H. C. Cheung, K. Asgari, C. L. Hampson, S. Body, C. M. Bradshaw, E. Szabadi, J. F. W. Deakin, I. M. Anderson, Effects of quinolinic acid-induced lesions of the nucleus accumbens core on inter-temporal choice: A quantitative analysis. *Psychopharmacology* **195**, 71–84 (2007).
34. S. E. Ahmari, T. Spellman, N. L. Douglass, M. A. Kheirbek, H. B. Simpson, K. Deisseroth, J. A. Gordon, R. Hen, Repeated cortico-striatal stimulation generates persistent OCD-like behavior. *Science* **340**, 1234–1239 (2013).
35. E. Burguière, P. Monteiro, G. Feng, A. M. Graybiel, Optogenetic stimulation of lateral orbitofronto-striatal pathway suppresses compulsive behaviors. *Science* **340**, 1243–1246 (2013).
36. S. L. Mondragón-González, C. Schreiweis, E. Burguière, Closed-loop recruitment of striatal interneurons prevents compulsive-like grooming behaviors. *Nat. Neurosci.* **27**, 1148–1156 (2024).
37. M. J. Ku, C. Y. Kim, J. W. Park, S. Lee, E. Y. Jeong, J.-W. Jeong, W. Y. Kim, J.-H. Kim, Wireless optogenetic stimulation on the prelimbic to the nucleus accumbens core circuit attenuates cocaine-induced behavioral sensitization. *Neurobiol. Dis.* **203**, 106733 (2024).
38. F. Ambroggi, A. Ishikawa, H. L. Fields, S. M. Nicola, Basolateral amygdala neurons facilitate reward-seeking behavior by exciting nucleus accumbens neurons. *Neuron* **59**, 648–661 (2008).
39. G. D. Stuber, D. R. Sparta, A. M. Stamatakis, W. A. van Leeuwen, J. E. Hardjoprajitno, S. Cho, K. M. Tye, K. A. Kempadoo, F. Zhang, K. Deisseroth, A. Bonci, Excitatory transmission from the amygdala to nucleus accumbens facilitates reward seeking. *Nature* **475**, 377–380 (2011).
40. A. Servonnet, P.-P. Rompré, A.-N. Samaha, Optogenetic activation of basolateral amygdala-to-nucleus accumbens core neurons promotes Pavlovian approach responses but not instrumental pursuit of reward cues. *Behav. Brain Res.* **440**, 114254 (2023).
41. V. Sturm, O. Fricke, C. P. Bührle, D. Lenartz, M. Maarouf, H. Treuer, J. K. Mai, G. Lehmkuhl, DBS in the basolateral amygdala improves symptoms of autism and related self-injurious behavior: A case report and hypothesis on the pathogenesis of the disorder. *Front. Hum. Neurosci.* **6**, 341 (2012).
42. T. J. Abel, B. D. Dalm, A. J. Grossbach, A. W. Jackson, T. Thomsen, J. D. W. Greenlee, Lateralized effect of pallidal stimulation on self-mutilation in Lesch-Nyhan disease. *J. Neurosurg. Pediatr.* **14**, 594–597 (2014).
43. V. Cojazzi, N. Innocenti, N. Castelli, V. Levi, V. Nazzi, A. Lozano, M. Rizzi, Posterior hypothalamic region deep brain stimulation for the treatment of aggression disorders in patients with intellectual disability: A systematic review. *Stereotact. Funct. Neurosurg.* **102**, 74–82 (2024).
44. H. Yan, L. M. Elkaim, F. Venetucci Gouveia, J. F. Huber, J. Germann, A. Loh, J. C. Benedetti-Isaac, P. K. Doshi, C. V. Torres, D. J. Segar, G. J. B. Elias, A. Boutet, G. R. Cosgrove, A. Fasano, A. M. Lozano, A. V. Kulkarni, G. M. Ibrahim, Deep brain stimulation for extreme behaviors associated with autism spectrum disorder converges on a common pathway: A systematic review and connectomic analysis. *J. Neurosurg.* **137**, 699–708 (2022).
45. K. Mithani, K. Zhang, H. Yan, L. Elkaim, P. J. Gariscsak, H. Suresh, F. V. Gouveia, A. Fasano, C. Gorodetsky, G. M. Ibrahim, Effect of deep brain stimulation on comorbid self-injurious behavior: A systematic review and meta-analysis of individual patient data. *Neuromodulation* **28**, 373–379 (2025).
46. C. Gorodetsky, K. Mithani, S. Breitbart, H. Yan, K. Zhang, F. V. Gouveia, N. Warsi, H. Suresh, S. M. Wong, J. Huber, E. N. Kerr, A. V. Kulkarni, M. J. Taylor, L. P. Hagopian, A. Fasano, G. M. Ibrahim, Deep brain stimulation of the nucleus accumbens for severe self-injurious behavior in children: A phase I pilot trial. *Biol. Psychiatry* **97**, 1116–1126 (2025).
47. J. L. Silverman, S. S. Tolu, C. L. Barkan, J. N. Crawley, Repetitive self-grooming behavior in the BTBR mouse model of autism is blocked by the mGluR5 antagonist MPEP. *Neuropsychopharmacology* **35**, 976–989 (2010).
48. A. V. Kalueff, A. M. Stewart, C. Song, K. C. Berridge, A. M. Graybiel, J. C. Fentress, Neurobiology of rodent self-grooming and its value for translational neuroscience. *Nat. Rev. Neurosci.* **17**, 45–59 (2016).
49. H. G. McFarlane, G. K. Kusek, M. Yang, J. L. Phoenix, V. J. Bolivar, J. N. Crawley, Autism-like behavioral phenotypes in BTBR T+tf/J mice. *Genes Brain Behav.* **7**, 152–163 (2008).
50. A. V. Kalueff, J. W. Aldridge, J. L. LaPorte, D. L. Murphy, P. Tuohimaa, Analyzing grooming microstructure in neurobehavioral experiments. *Nat. Protoc.* **2**, 2538–2544 (2007).
51. B. L. Pearson, R. L. H. Pobbe, E. B. Defensor, L. Oasay, V. J. Bolivar, D. C. Blanchard, R. J. Blanchard, Motor and cognitive stereotypies in the BTBR T+tf/J mouse model of autism. *Genes Brain Behav.* **10**, 228–235 (2011).
52. M. P. Leussis, V. J. Bolivar, Habituation in rodents: A review of behavior, neurobiology, and genetics. *Neurosci. Biobehav. Rev.* **30**, 1045–1064 (2006).
53. F. Iannello, Non-intrusive high throughput automated data collection from the home cage. *Heliyon* **5**, e01454 (2019).
54. B. J. Nieman, M. C. van Eede, S. Spring, J. Dazai, R. M. Henkelman, J. P. Lerch, MRI to assess neurological function. *Curr. Protoc. Mouse Biol.* **8**, e44 (2018).
55. A. E. Dorr, J. P. Lerch, S. Spring, N. Kabani, R. M. Henkelman, High resolution three-dimensional brain atlas using an average magnetic resonance image of 40 adult C57Bl/6J mice. *Neuroimage* **42**, 60–69 (2008).
56. G. Kohls, M. Schulte-Rüther, B. Nehrkorn, K. Müller, G. R. Fink, I. Kamp-Becker, B. Herpertz-Dahlmann, R. T. Schultz, K. Konrad, Reward system dysfunction in autism spectrum disorders. *Soc. Cogn. Affect. Neurosci.* **8**, 565–572 (2013).
57. J. W. Bodfish, F. J. Symons, D. E. Parker, M. H. Lewis, Repetitive behavior scale–revised, American Psychological Association (APA) (2014); https://doi.org/10.1037/t17338-000.
58. A. Horn, A. A. Kühn, Lead-DBS: A toolbox for deep brain stimulation electrode localizations and visualizations. *Neuroimage* **107**, 127–135 (2015).
59. G. J. B. Elias, J. Germann, S. E. Joel, N. Li, A. Horn, A. Boutet, A. M. Lozano, A large normative connectome for exploring the tractographic correlates of focal brain interventions. *Sci. Data* **11**, 353 (2024).
60. N. van Meer, A. C. Houtman, P. Van Schuerbeek, T. Vanderhasselt, C. Milleret, M. P. Ten Tusscher, Interhemispheric connections between the primary visual cortical

areas via the anterior commissure in human callosal agenesis. *Front. Syst. Neurosci.* **10**, 101 (2016).
61. G. J. B. Elias, P. Giacobbe, A. Boutet, J. Germann, M. E. Beyn, R. M. Gramer, A. Pancholi, S. E. Joel, A. M. Lozano, Probing the circuitry of panic with deep brain stimulation: Connectomic analysis and review of the literature. *Brain Stimul.* **13**, 10–14 (2020).
62. J. Germann, G. J. B. Elias, C. Neudorfer, A. Boutet, C. T. Chow, E. H. Y. Wong, R. Parmar, F. V. Gouveia, A. Loh, P. Giacobbe, S. J. Kim, H. H. Jung, V. Bhat, W. Kucharczyk, J. W. Chang, A. M. Lozano, Potential optimization of focused ultrasound capsulotomy for obsessive compulsive disorder. *Brain* **144**, 3529–3540 (2021).
63. A. Di Martino, C. Kelly, R. Grzadzinski, X.-N. Zuo, M. Mennes, M. A. Mairena, C. Lord, F. X. Castellanos, M. P. Milham, Aberrant striatal functional connectivity in children with autism. *Biol. Psychiatry* **69**, 847–856 (2011).
64. J. Germann, F. V. Gouveia, M. M. Chakravarty, G. A. Devenyi, Longitudinal deformation-based morphometry pipeline to study neuroanatomical differences in structural MRI based on SyN unbiased templates. *Aperture Neuro* **5**, 10.52294/001c.133510 (2025).
65. D. W. Yip, A. O. Awosika, F. Lui, "Physiology, motor cortical" in *StatPearls* (StatPearls Publishing, 2024).
66. R. L. Buckner, The cerebellum and cognitive function: 25 years of insight from anatomy and neuroimaging. *Neuron* **80**, 807–815 (2013).
67. E. M. Aminoff, K. Kveraga, M. Bar, The role of the parahippocampal cortex in cognition. *Trends Cogn. Sci.* **17**, 379–390 (2013).
68. I. R. Olson, A. Plotzker, Y. Ezzyat, The enigmatic temporal pole: A review of findings on social and emotional processing. *Brain* **130**, 1718–1731 (2007).
69. R. Zhang, H. Deng, X. Xiao, The insular cortex: An interface between sensation, emotion and cognition. *Neurosci. Bull.* **40**, 1763–1773 (2024).
70. M. M. Behbehani, Functional characteristics of the midbrain periaqueductal gray. *Prog. Neurobiol.* **46**, 575–605 (1995).
71. F. J. Symons, T. Thompson, Self-injurious behaviour and body site preference. *J. Intellect. Disabil. Res.* **41**, 456–468 (1997).
72. K. M. Newell, J. H. Challis, R. L. Boros, J. W. Bodfish, Further evidence on the dynamics of self-injurious behaviors: Impact forces and limb motions. *Am. J. Ment. Retard.* **107**, 60–68 (2002).
73. J. Ellegood, B. A. Babineau, R. M. Henkelman, J. P. Lerch, J. N. Crawley, Neuroanatomical analysis of the BTBR mouse model of autism using magnetic resonance imaging and diffusion tensor imaging. *Neuroimage* **70**, 288–300 (2013).
74. W. Sato, Y. Kubota, T. Kochiyama, S. Uono, S. Yoshimura, R. Sawada, M. Sakihama, M. Toichi, Increased putamen volume in adults with autism spectrum disorder. *Front. Hum. Neurosci.* **8**, 957 (2014).
75. J. D. Salamone, M. Correa, S. M. Mingote, S. M. Weber, Beyond the reward hypothesis: Alternative functions of nucleus accumbens dopamine. *Curr. Opin. Pharmacol.* **5**, 34–41 (2005).
76. J. D. Salamone, M. Correa, Motivational views of reinforcement: Implications for understanding the behavioral functions of nucleus accumbens dopamine. *Behav. Brain Res.* **137**, 3–25 (2002).
77. F. Furniss, A. B. Biswas, "Neurobiology of self-injurious behavior" in *Self-Injurious Behavior in Individuals with Neurodevelopmental Conditions* (Springer International Publishing, 2020), pp. 51–110.
78. S. Lammel, B. K. Lim, C. Ran, K. W. Huang, M. J. Betley, K. M. Tye, K. Deisseroth, R. C. Malenka, Input-specific control of reward and aversion in the ventral tegmental area. *Nature* **491**, 212–217 (2012).
79. J. E. Markowitz, W. F. Gillis, M. Jay, J. Wood, R. W. Harris, R. Cieszkowski, R. Scott, D. Brann, D. Koveal, T. Kula, C. Weinreb, M. A. M. Osman, S. R. Pinto, N. Uchida, S. W. Linderman, B. L. Sabatini, S. R. Datta, Spontaneous behaviour is structured by reinforcement without explicit reward. *Nature* **614**, 108–117 (2023).
80. H.-C. Tsai, F. Zhang, A. Adamantidis, G. D. Stuber, A. Bonci, L. de Lecea, K. Deisseroth, Phasic firing in dopaminergic neurons is sufficient for behavioral conditioning. *Science* **324**, 1080–1084 (2009).
81. S. Naze, L. J. Hearne, J. A. Roberts, P. Sanz-Leon, B. Burgher, C. Hall, S. Sonkusare, Z. Nott, L. Marcus, E. Savage, C. Robinson, Y. E. Tian, A. Zalesky, M. Breakspear, L. Cocchi, Mechanisms of imbalanced frontostriatal functional connectivity in obsessive-compulsive disorder. *Brain* **146**, 1322–1327 (2023).
82. D. Denys, M. Mantione, M. Figee, P. van den Munckhof, F. Koerselman, H. Westenberg, A. Bosch, R. Schuurman, Deep brain stimulation of the nucleus accumbens for treatment-refractory obsessive-compulsive disorder. *Arch. Gen. Psychiatry* **67**, 1061–1068 (2010).
83. M. Figee, J. Luigjes, R. Smolders, C.-E. Valencia-Alfonso, G. van Wingen, B. de Kwaasteniet, M. Mantione, P. Ooms, P. de Koning, N. Vulink, N. Levar, L. Droge, P. van den Munckhof, P. R. Schuurman, A. Nederveen, W. van den Brink, A. Mazaheri, M. Vink, D. Denys, Deep brain stimulation restores frontostriatal network activity in obsessive-compulsive disorder. *Nat. Neurosci.* **16**, 386–387 (2013).
84. L. Cerliani, M. Mennes, R. M. Thomas, A. Di Martino, M. Thioux, C. Keysers, Increased functional connectivity between subcortical and cortical resting-state networks in autism spectrum disorder. *JAMA Psychiatry* **72**, 767–777 (2015).
85. C. J. Honey, J.-P. Thivierge, O. Sporns, Can structure predict function in the human brain? *Neuroimage* **52**, 766–776 (2010).
86. W. Groen, M. Teluij, J. Buitelaar, I. Tendolkar, Amygdala and hippocampus enlargement during adolescence in autism. *J. Am. Acad. Child Adolesc. Psychiatry* **49**, 552–560 (2010).
87. J. Ellegood, E. Anagnostou, B. A. Babineau, J. N. Crawley, L. Lin, M. Genestine, E. DiCicco-Bloom, J. K. Y. Lai, J. A. Foster, O. Peñagarikano, D. H. Geschwind, L. K. Pacey, D. R. Hampson, C. L. Laliberté, A. A. Mills, E. Tam, L. R. Osborne, M. Kouser, F. Espinosa-Becerra, Z. Xuan, C. M. Powell, A. Raznahan, D. M. Robins, N. Nakai, J. Nakatani, T. Takumi, M. C. van Eede, T. M. Kerr, C. Muller, R. D. Blakely, J. Veenstra-VanderWeele, R. M. Henkelman, J. P. Lerch, Clustering autism: Using neuroanatomical differences in 26 mouse models to gain insight into the heterogeneity. *Mol. Psychiatry* **20**, 118–125 (2015).
88. A. Estes, D. W. W. Shaw, B. F. Sparks, S. Friedman, J. N. Giedd, G. Dawson, M. Bryan, S. R. Dager, Basal ganglia morphometry and repetitive behavior in young children with autism spectrum disorder. *Autism Res.* **4**, 212–220 (2011).
89. D. Gallino, G. A. Devenyi, J. Germann, E. Guma, C. Anastassiadis, M. M. Chakravarty, Longitudinal assessment of the neuroanatomical consequences of deep brain stimulation: Application of fornical DBS in an Alzheimer's mouse model. *Brain Res.* **1715**, 213–223 (2019).
90. M. M. Chakravarty, C. Hamani, A. Martinez-Canabal, J. Ellegood, C. Laliberté, J. N. Nobrega, T. Sankar, A. M. Lozano, P. W. Frankland, J. P. Lerch, Deep brain stimulation of the ventromedial prefrontal cortex causes reorganization of neuronal processes and vasculature. *Neuroimage* **125**, 422–427 (2016).
91. S. S. Kaae, F. Chen, G. Wegener, T. M. Madsen, J. R. Nyengaard, Quantitative hippocampal structural changes following electroconvulsive seizure treatment in a rat model of depression. *Synapse* **66**, 667–676 (2012).
92. F. Chen, T. M. Madsen, G. Wegener, J. R. Nyengaard, Repeated electroconvulsive seizures increase the total number of synapses in adult male rat hippocampus. *Eur. Neuropsychopharmacol.* **19**, 329–338 (2009).
93. H. Hotta, K. Masamoto, S. Uchida, Y. Sekiguchi, H. Takuwa, H. Kawaguchi, K. Shigemoto, R. Sudo, K. Tanishita, H. Ito, I. Kanno, Layer-specific dilation of penetrating arteries induced by stimulation of the nucleus basalis of Meynert in the mouse frontal cortex. *J. Cereb. Blood Flow Metab.* **33**, 1440–1447 (2013).
94. A. E. Pohodich, H. Yalamanchili, A. T. Raman, Y.-W. Wan, M. Gundry, S. Hao, H. Jin, J. Tang, Z. Liu, H. Y. Zoghbi, Forniceal deep brain stimulation induces gene expression and splicing changes that promote neurogenesis and plasticity. *eLife* **7**, e34031 (2018).
95. N. Yan, N. Chen, H. Zhu, J. Zhang, M. Sim, Y. Ma, W. Wang, High-frequency stimulation of nucleus accumbens changes in dopaminergic reward circuit. *PLOS ONE* **8**, e79318 (2013).
96. W.-H. Hu, Y.-F. Bi, K. Zhang, F.-G. Meng, J.-G. Zhang, High-frequency electrical stimulation in the nucleus accumbens of morphine-treated rats suppresses neuronal firing in reward-related brain regions. *Med. Sci. Monit.* **17**, BR153-60 (2011).
97. N. Wei, Y. Wang, X. Wang, Z. He, M. Zhang, X. Zhang, Y. Pan, J. Zhang, Z. Qin, K. Zhang, The different effects of high-frequency stimulation of the nucleus accumbens shell and core on food consumption are possibly associated with different neural responses in the lateral hypothalamic area. *Neuroscience* **301**, 312–322 (2015).
98. H. Zhou, J. Zhu, J. Jia, W. Xiang, H. Peng, Y. Zhang, B. Liu, Y. Mu, Y. Lu, The antidepressant effect of nucleus accumbens deep brain stimulation is mediated by parvalbumin-positive interneurons in the dorsal dentate gyrus. *Neurobiol. Stress* **21**, 100492 (2022).
99. C. Schmuckermair, S. Gaburro, A. Sah, R. Landgraf, S. B. Sartori, N. Singewald, Behavioral and neurobiological effects of deep brain stimulation in a mouse model of high anxiety- and depression-like behavior. *Neuropsychopharmacology* **38**, 1234–1244 (2013).
100. A. van Dijk, A. A. Klompmakers, M. G. P. Feenstra, D. Denys, Deep brain stimulation of the accumbens increases dopamine, serotonin, and noradrenaline in the prefrontal cortex. *J. Neurochem.* **123**, 897–903 (2012).
101. H. Shibata, J. Naito, Organization of anterior cingulate and frontal cortical projections to the anterior and laterodorsal thalamic nuclei in the rat. *Brain Res.* **1059**, 93–103 (2005).
102. M. N. Baliki, A. Mansour, A. T. Baria, L. Huang, S. E. Berger, H. L. Fields, A. V. Apkarian, Parceling human accumbens into putative core and shell dissociates encoding of values for reward and pain. *J. Neurosci.* **33**, 16383–16393 (2013).
103. M. N. Baliki, P. Y. Geha, H. L. Fields, A. V. Apkarian, Predicting value of pain and analgesia: Nucleus accumbens response to noxious stimuli changes in the presence of chronic pain. *Neuron* **66**, 149–160 (2010).
104. M. C. Schippers, B. Bruinsma, M. Gaastra, T. I. Mesman, D. Denys, T. J. De Vries, T. Pattij, Deep brain stimulation of the nucleus accumbens core affects trait impulsivity in a baseline-dependent manner. *Front. Behav. Neurosci.* **11**, 52 (2017).
105. G. Di Chiara, Nucleus accumbens shell and core dopamine: Differential role in behavior and addiction. *Behav. Brain Res.* **137**, 75–114 (2002).
106. C. V. Torres Díaz, S. Treu, B. Strange, M. Lara, M. Navas, E. Ezquiaga, E. S. Zazo, J. S. Vicente, I. Muñiz, F. S. Fernandez, Deep brain stimulation of the nucleus accumbens, ventral striatum, or internal capsule targets for medication-resistant obsessive-compulsive disorder: A multicenter study. *World Neurosurg.* **155**, e168–e176 (2021).

107. T. Schüller, S. Kohl, T. Dembek, M. Tittgemeyer, D. Huys, V. Visser-Vandewalle, N. Li, L. Wehmeyer, M. Barbe, J. Kuhn, J. C. Baldermann, Internal capsule/nucleus accumbens deep brain stimulation increases impulsive decision making in obsessive-compulsive disorder. *Biol. Psychiatry Cogn. Neurosci. Neuroimaging* **8**, 281–289 (2023).
108. M. H. Histed, V. Bonin, R. C. Reid, Direct activation of sparse, distributed populations of cortical neurons by electrical microstimulation. *Neuron* **63**, 508–522 (2009).
109. N. J. Michelson, J. R. Eles, A. L. Vazquez, K. A. Ludwig, T. D. Y. Kozai, Calcium activation of cortical neurons by continuous electrical stimulation: Frequency dependence, temporal fidelity, and activation density. *J. Neurosci. Res.* **97**, 620–638 (2019).
110. Z. H. T. Kiss, D. M. Mooney, L. Renaud, B. Hu, Neuronal response to local electrical stimulation in rat thalamus: Physiological implications for mechanisms of deep brain stimulation. *Neuroscience* **113**, 137–143 (2002).
111. T. Boraud, E. Bezard, B. Bioulac, C. Gross, High frequency stimulation of the internal Globus Pallidus (GPi) simultaneously improves parkinsonian symptoms and reduces the firing frequency of GPi neurons in the MPTP-treated monkey. *Neurosci. Lett.* **215**, 17–20 (1996).
112. A. Benazzouz, M. Hallett, Mechanism of action of deep brain stimulation. *Neurology* **55**, S13–S16 (2000).
113. Y. Shi, M. Wang, L. Xiao, L. Gui, W. Zheng, L. Bai, B. Su, B. Li, Y. Xu, W. Pan, J. Zhang, W. Wang, Potential therapeutic mechanism of deep brain stimulation of the nucleus accumbens in obsessive-compulsive disorder. *Front. Cell. Neurosci.* **16**, 1057887 (2022).
114. B. J. G. van den Boom, A. Elhazaz-Fernandez, P. A. Rasmussen, E. H. van Beest, A. Parthasarathy, D. Denys, I. Willuhn, Unraveling the mechanisms of deep brain stimulation of the internal capsule in a mouse model. *Nat. Commun.* **14**, 5385 (2023).
115. C. C. McIntyre, W. M. Grill, Excitation of central nervous system neurons by nonuniform electric fields. *Biophys. J.* **76**, 878–888 (1999).
116. L. G. Nowak, J. Bullier, Axons, but not cell bodies, are activated by electrical stimulation in cortical gray matter. II. Evidence from selective inactivation of cell bodies and axon initial segments. *Exp. Brain Res.* **118**, 489–500 (1998).
117. J. L. Vitek, Mechanisms of deep brain stimulation: Excitation or inhibition. *Mov. Disord.* **17**, S69–S72 (2002).
118. C. C. McIntyre, W. M. Grill, D. L. Sherman, N. V. Thakor, Cellular effects of deep brain stimulation: Model-based analysis of activation and inhibition. *J. Neurophysiol.* **91**, 1457–1469 (2004).
119. Q. Wang, H. Akram, M. Muthuraman, G. Gonzalez-Escamilla, S. A. Sheth, S. Oxenford, F.-C. Yeh, S. Groppa, N. Vanegas-Arroyave, L. Zrinzo, N. Li, A. Kühn, A. Horn, Normative vs. patient-specific brain connectivity in deep brain stimulation. *Neuroimage* **224**, 117307 (2021).
120. R. M. J. Deacon, Digging and marble burying in mice: Simple methods for in vivo identification of biological impacts. *Nat. Protoc.* **1**, 122–124 (2006).
121. A.-K. Kraeuter, P. C. Guest, Z. Sarnyai, The open field test for measuring locomotor activity and anxiety-like behavior. *Methods Mol. Biol.* **1916**, 99–103 (2019).
122. M. Yang, J. L. Silverman, J. N. Crawley, Automated three-chambered social approach task for mice. *Curr. Protoc. Neurosci.*, 10.1002/0471142301.ns0826s56 **8**, Unit 8.26 (2011).
123. L. S. Cahill, C. L. Laliberté, J. Ellegood, S. Spring, J. A. Gleave, M. C. van Eede, J. P. Lerch, R. M. Henkelman, Preparation of fixed mouse brains for MRI. *Neuroimage* **60**, 933–939 (2012).
124. N. Percie du Sert, V. Hurst, A. Ahluwalia, S. Alam, M. T. Avey, M. Baker, W. J. Browne, A. Clark, I. C. Cuthill, U. Dirnagl, M. Emerson, P. Garner, S. T. Holgate, D. W. Howells, N. A. Karp, S. E. Lazic, K. Lidster, C. J. MacCallum, M. Macleod, E. J. Pearl, O. H. Petersen, F. Rawle, P. Reynolds, K. Rooney, E. S. Sena, S. D. Silberberg, T. Steckler, H. Würbel, The ARRIVE guidelines 2.0: Updated guidelines for reporting animal research. *PLoS Biol.* **18**, e3000410 (2020).
125. H. Yan, L. Siegel, S. Breitbart, C. Gorodetsky, A. Fasano, A. Rahim, A. Loh, A. V. Kulkarni, G. M. Ibrahim, An open-label prospective pilot trial of nucleus accumbens deep brain stimulation for children with autism spectrum disorder and severe, refractory self-injurious behavior: Study protocol. *Pilot Feasibility Stud.* **8**, 24 (2022).
126. G. J. B. Elias, A. Boutet, S. E. Joel, J. Germann, D. Gwun, C. Neudorfer, R. M. Gramer, M. Algarni, V. Paramanandam, S. Prasad, M. E. Beyn, A. Horn, R. Madhavan, M. Ranjan, C. S. Lozano, A. A. Kühn, J. Ashe, W. Kucharczyk, R. P. Munhoz, P. Giacobbe, S. H. Kennedy, D. B. Woodside, S. K. Kalia, A. Fasano, M. Hodaie, A. M. Lozano, Probabilistic mapping of deep brain stimulation: Insights from 15 years of therapy. *Ann. Neurol.* **89**, 426–443 (2021).
127. D. L. Collins, P. Neelin, T. M. Peters, A. C. Evans, Automatic 3D intersubject registration of MR volumetric data in standardized Talairach space. *J. Comput. Assist. Tomogr.* **18**, 192–205 (1994).
128. B. B. Avants, C. L. Epstein, M. Grossman, J. C. Gee, Symmetric diffeomorphic image registration with cross-correlation: Evaluating automated labeling of elderly and neurodegenerative brain. *Med. Image Anal.* **12**, 26–41 (2008).
129. B. B. Avants, N. J. Tustison, G. Song, P. A. Cook, A. Klein, J. C. Gee, A reproducible evaluation of ANTs similarity metric performance in brain image registration. *Neuroimage* **54**, 2033–2044 (2011).
130. R. W. Cox, AFNI: Software for analysis and visualization of functional magnetic resonance neuroimages. *Comput. Biomed. Res.* **29**, 162–173 (1996).
131. S. D. Forman, J. D. Cohen, M. Fitzgerald, W. F. Eddy, M. A. Mintun, D. C. Noll, Improved assessment of significant activation in functional magnetic resonance imaging (fMRI): Use of a cluster-size threshold. *Magn. Reson. Med.* **33**, 636–647 (1995).
132. Reference Atlas :: Allen Brain Atlas: Mouse Brain. https://mouse.brain-map.org/static/atlas.
133. R. Bakker, P. Tiesinga, R. Kötter, The Scalable Brain Atlas: Instant web-based access to public brain atlases and related content. *Neuroinformatics* **13**, 353–366 (2015).
134. G. Paxinos, K. B. J. Franklin, *Paxinos and Franklin's the Mouse Brain in Stereotaxic Coordinates* (Academic Press, 2019).
135. C. Gorodetsky, A. Fasano, Basic tips: How do I start programming deep brain stimulation in Parkinson disease patients? *Mov. Disord. Clin. Pract.* **8**, 639–644 (2021).
136. K. K. Zhang, R. Matin, C. Gorodetsky, G. M. Ibrahim, F. V. Gouveia, Systematic review of rodent studies of deep brain stimulation for the treatment of neurological, developmental and neuropsychiatric disorders. *Transl. Psychiatry* **14**, 186 (2024).
137. J. L. Silverman, M. Yang, C. Lord, J. N. Crawley, Behavioural phenotyping assays for mouse models of autism. *Nat. Rev. Neurosci.* **11**, 490–502 (2010).
138. R. Müller, R. Bravo, J. Burckhardt, T. Curran, Induction of c-fos gene and protein by growth factors precedes activation of c-myc. *Nature* **312**, 716–720 (1984).
139. T. Schulte, S. Brecht, T. Herdegen, M. Illert, H. M. Mehdorn, W. Hamel, Induction of immediate early gene expression by high-frequency stimulation of the subthalamic nucleus in rats. *Neuroscience* **138**, 1377–1385 (2006).
140. A. Fomenko, D. J. Lee, C. McKinnon, E. J. Lee, M. L. de Snoo, E. Gondard, C. Neudorfer, C. Hamani, A. M. Lozano, L. V. Kalia, S. K. Kalia, Deep brain stimulation of the medial septal nucleus induces expression of a virally delivered reporter gene in Dentate Gyrus. *Front. Neurosci.* **14**, 463 (2020).
141. A. Saryyeva, M. Nakamura, J. K. Krauss, K. Schwabe, c-Fos expression after deep brain stimulation of the pedunculopontine tegmental nucleus in the rat 6-hydroxydopamine Parkinson model. *J. Chem. Neuroanat.* **42**, 210–217 (2011).
142. J. P. Lerch, J. G. Sled, R. M. Henkelman, MRI phenotyping of genetically altered mice. *Methods Mol. Biol.* **711**, 349–361 (2011).
143. J. P. Lerch, L. Gazdzinski, J. Germann, J. G. Sled, R. M. Henkelman, B. J. Nieman, Wanted dead or alive? The tradeoff between in-vivo versus ex-vivo MR brain imaging in the mouse. *Front. Neuroinform.* **6**, 6 (2012).
144. K. J. Friston, *Statistical Parametric Mapping: The Analysis of Funtional Brain Images* (2007).
145. S. Ewert, P. Plettig, N. Li, M. M. Chakravarty, D. L. Collins, T. M. Herrington, A. A. Kühn, A. Horn, Toward defining deep brain stimulation targets in MNI space: A subcortical atlas based on multimodal MRI, histology and structural connectivity. *Neuroimage* **170**, 271–282 (2018).
146. A. Horn, N. Li, T. A. Dembek, A. Kappel, C. Boulay, S. Ewert, A. Tietze, A. Husch, T. Perera, W.-J. Neumann, M. Reisert, H. Si, R. Oostenveld, C. Rorden, F.-C. Yeh, Q. Fang, T. M. Herrington, J. Vorwerk, A. A. Kühn, Lead-DBS v2: Towards a comprehensive pipeline for deep brain stimulation imaging. *Neuroimage* **184**, 293–316 (2019).

Acknowledgments

Funding: This work was supported by a catalyst grant from the Garry Hurvitz Centre for Brain and Mental Health at the Hospital for Sick Children and the Abe Bresver Chair in Functional Neurosurgery (to G.M.I.). **Author contributions:** Conceptualization: K.Z., J.G., J.P.L., B.J.N., S.B., A.F., F.V.G., and G.M.I. Data curation: K.Z., J.G., K.M., H.S., F.V.G., and G.M.I. Formal analysis: K.Z., J.G., K.M., J.E., H.S., F.V.G., and G.M.I. Funding acquisition: G.M.I. Investigation: K.Z., J.G., R.M., K.M., J.E., S.B., A.F., F.V.G., and G.M.I. Methodology: K.Z., J.G., J.E., J.P.L., A.F., F.V.G., and G.M.I. Project administration: K.Z., F.V.G., and G.M.I. Resources: K.Z., B.J.N., M.J.T., F.V.G., and G.M.I. Software: K.Z., J.E., F.V.G., and G.M.I. Supervision: A.F., F.V.G., and G.M.I. Validation: K.Z., J.G., R.M., F.V.G., and G.M.I. Visualization: K.Z., J.G., H.S., S.W., F.V.G., and G.M.I. Writing—original draft: K.Z., F.V.G., and G.M.I. Writing—review and editing: K.Z., J.G., K.M., J.E., H.S., S.W., J.P.L., B.J.N., M.J.T., S.B., A.F., C.G., F.V.G., and G.M.I. **Competing interests:** C.G., A.F., and G.M.I. receive consulting or advisory fees from Medtronic Inc. A.F. also received consulting and speaking fees from Boston Scientific and Abbott. G.M.I. also reports a relationship with Synergia Inc. and LivaNova Inc. that includes consulting and advisory fees and investigator-initiated funding. These organizations played no role in any part of this study, including its design, conduct, analysis, or writing. All other authors declare that they have no biomedical financial interests or potential competing interests. **Data, code, and materials availability:** All data and code needed to evaluate and reproduce the results in the paper are present in the paper and/or the Supplementary Materials. Code for electrode localization, modeling of the volume of activated tissue, and imaging connectomics are freely available in Lead-DBS (https://lead-dbs.org/). Structural (https://doi.org/10.1038/s41597-024-03197-0) and functional (https://doi.org/10.7910/DVN/KKTJQC) connectomes are publicly available. The code used for data-processing and human deformation-based morphometry analysis are available at http://dx.doi.org/10.52294/001c.133510, https://github.com/CoBrALab/twolevel_ants_dbm, and https://github.com/CoBrALab/optimized_antsMultivariateTemplateConstruction. This study did not generate new materials.

Submitted 18 August 2025
Accepted 11 March 2026
Published 10 April 2026
10.1126/sciadv.aeb5842